Signaling and Propagation Modes in Highpass and Bandpass Neural Network Columns Constructed From Eckhorn Neurons

Richard B. Wells[1], Tianlai Lu[2], and Tim Montoya[3]

The MRC Institute

BEL 316

University of Idaho

Moscow, ID 83844-1024

Jan. 8, 2006

[1]The author is with the MRC Institute, University of Idaho.

[2]The author was with the MRC Institute. He is now at Rice University.

[3]The author was with the MRC Institute. He is now at the University of Idaho.

Corresponding Author:

Richard B. Wells, Ph.D.
Telephone: (208) 885-4353
Fax: (208) 885-6840
email: rwells@mrc.uidaho.edu

Abstract

Novel frequency-selective recurrent neural networks constructed from Eckhorn's neuron model are described and a simple and precise theory of their operation is given. The networks are organized in basic cell groups, and larger networks are constructed by interconnecting these groups. Individual groups are modeled along the lines of the columnar organization of connectivity reported for neocortex. The cell groups are designed to be pulse rate selective "highpass filters". "Bandpass filters", i.e. assemblies that respond over a specific range of synchronous input pulse rates, are realized using pairs of highpass structures connected in a feedback arrangement. Signal propagation in chains of these networks is studied and certain interesting neurodynamics are described and explained. These include wave and packet generation and propagation characteristics, a rate-multiplier effect, evanescent wave propagation, dipulse propagation, and subharmonic, harmonic and anharmonic spectrum generation by these networks.

Keywords: cell group, cell assembly, functional column, synchronized signaling, neural network.

1. Introduction

In this paper we examine the signaling, signal propagation, and synchronization properties of a class of frequency-selective neural network cell groups and cell assemblies. To the best of our knowledge, the neural network topology presented in this paper has not been previously reported. The motivation for this study was to better understand signaling and wave generation and propagation phenomena in different frequency bands for neocortex that has been reported in recent years in numerous journal papers. In particular we are interested in how different signaling frequencies, i.e. alpha-band (7-14 Hz), beta-band (14-28 Hz), and gamma-band (28-70 Hz), arise in neocortex and why these different frequency bands exhibit such radically different characteristic propagation distances. It is presently thought that alpha- and beta-band signals are localized, whereas gamma-band signals have been shown to propagate with a relatively high degree of tight correlation coupling over distances from a few millimeters up to approximately 1 cm, and to propagate for even greater distances but with loss of correlation coupling in neocortex.

Recently Bruns and Eckhorn (2003) reported some interesting statistical coupling results between gamma-band signals and low-frequency signals (0 to 3.5 Hz). Although it was not our original intent to explore this low-frequency region, in the course of this study we observed the spontaneous production of spectral components in this frequency band. The mechanism for its production by the networks reported here differs from the mechanism recently postulated by Eckhorn et al. (2004), although nothing in our study offers any basis to suggest their mechanism hypothesis is contradicted by our findings. The mechanism we observed also differs from another reported by Anderson et al. (2000). Our view is that there are probably many mechanisms by which low-frequency signals are produced; we merely propose to add

another putative mechanism to the list.

The greater majority of theoretical studies on synchronized signal propagation have focused mainly on gamma-band signaling specifically or mono-frequency signaling in general. Mathematical research into fundamental neurodynamic properties often use highly abstract "neurons" such as the phase-model oscillator for loosely coupled assemblies (Kuramoto, 1987; Schuster and Wagner, 1990; Wang, 1995) or some variant of the Fitzhugh-Nagumo or Morris-Lecar models for strongly coupled assemblies (Terman and Wang, 1995; Campbell et al., 2004; Medvedev and Kopell, 2001). Studies such as these uncover useful mathematical information on the characteristics of systems of coupled oscillators, but the reductionist pathway from these findings to biological neural networks is often unclear.

Coming from the other direction are simulation studies of networks based on commonly used simplified neuron models such as the leaky integrate-and-fire neuron (Campbell et al., 1999; Bressloff, 1999; Ermentrout, 1998), the theta neuron (Ermentrout and Kopell, 1986; Osan et al., 2002), the Rulkov family of neuron models (Rulkov et al., 2004), and other biologically-inspired models (Rinzel et al., 1998; Terman et al., 2001). These simulation studies provide a great deal of empirical information about traveling wave and synchrony properties. On the other hand, these findings tend to be emergent properties of the networks used in the simulations. Because of the general homogeneity of the network topologies it is often the case that, to use a simile, the results are like the emergent properties of crystalline solids: Important properties are found *ex post facto* but it is difficult to extrapolate and predict what will happen when the network topology and/or the properties of its constituent neurons is/are significantly altered. To borrow some engineering terminology, general *design rules* for neural networks are often not made evident through the reported findings.

In this study we developed neural cell group structures with a mind to being able to then develop neural assemblies composed of these basic cell groups, and then larger networks, constructed as networks of assemblies, in a hierarchal fashion. This tactic is suggested by the fact that the neocortex is known to be organized around functional columns and by the possibility that simpler cell group structures would have more easily apprehensible design guidelines from an examination of the basic equations that govern the actions of the neurons within it. On the whole this expectation has not been disappointed, although it is also true that even with these networks we encountered some interesting emergent properties we had not predicted in advance. In the balance against these surprises, however, was an easier task of analyzing what produced these behaviors in the network. This proved useful in making modifications to our networks in pursuit of desired properties in its behavior.

The topology and connectivity in our fundamental cell group was inspired by a recent review of connectivity within the neocortex (Douglas and Martin, 2004). Our cell group is a layered structure of "kernels" more or less corresponding to cortical layers 2/3 (L-III), 4 (L-IV), 5 (L-V), and 6 (L-VI) of neocortex. Each kernel contains a 4:1 ratio of excitatory to inhibitory neurons, which more or less corresponds to the relative populations in neocortex. In this paper all the kernels are comprised of four excitatory neurons and one inhibitory neuron, which is the minimum size consistent with the desired ratio. A cell group consists of six kernels (30 neurons/group). With one exception to be discussed later, the inhibitory neuron projects only to the excitatory neurons within its kernel. These are the structural constraints we imposed in order that we might find it easier in later studies to relate the network model properties to biological networks. We define a "functional column" to consist of either a single cell group or a cell assembly composed of two or more cell groups with each cell group in reciprocal

interaction with the others via fixed “input” and “output” pathways from specified kernels in each. Cell groups assembled to form a functional column typically have different neuronal parameters and different properties. In this paper the largest functional column is comprised of two non-identical cell groups. Functional columns are interconnected to form larger cell assemblies, and each functional column has a pre-specified input pathway (“input port”) and output pathway (“output port”). In this paper we only report on functional column networks comprised of identical functional columns organized into serial chains. This is because here our purpose is to examine signal generation and propagation characteristics in one direction in these chains. Furthermore, this study is restricted to signaling dynamics between adjacent “patches” and not with longer distance cortico-cortical signaling nor with recurrent feedback from downstream columns back into upstream columns.

Although our original studies followed rather closely the laminar and intra-areal topology reviewed by Douglas and Martin (2004), we soon found that the highly synchronized firing patterns we were observing in our networks made it mathematically possible to use a somewhat different network structure. This structure, reported here, we found to be more amenable to an analysis of its dynamics. We think it is mathematically equivalent in its input-output dynamics to our earlier structures, although we have not developed a formal proof of this.

We chose the Eckhorn neuron model (Eckhorn et al., 1990) because of its ability to produce synchronized firing patterns, the ease with which its frequency-response and output firing pattern characteristics can be designed and altered, and because networks constructed from these neurons are known to be able to produce and support wave propagation phenomena (Johnson and Ritter, 1993). The Eckhorn neuron is comprised of a “spike encoder” output section (often called a “soma”; however, we will use the term “neuromime” for this function in

this paper) and one or more synaptic input sections called “dendrites” which provide the input to the neuromime compartment.

An Eckhorn dendrite has two types of input pathways. The direct data pathway is called the feeding field input. The other pathway is called the linking field input, and this pathway gives Eckhorn networks their synchronizing property. In our network each excitatory neuron has two dendrites, one for excitatory inputs and another for inhibitory inputs. The excitatory dendrite has both the feeding field and linking field inputs, and each of these pathways contains a leaky integrator with a specified time constant (τ_{fe} for the feeding field and τ_{λ} for the linking field). Synaptic inputs are weighted and summed and then applied to their respective integrators. The inhibitory dendrite contains only a feeding field pathway and its integrator is characterized by time constant τ_{fi}. The output of the inhibitory dendrite is subtracted from the output of the excitatory dendrite and the result is fed to the neuromime. The neuromime is characterized by a variable-threshold time constant τ_s, a baseline firing threshold θ_0, and a refractory time factor V_s.

Our inhibitory neurons are similar except that they have only an excitatory dendrite and this dendrite lacks the linking field pathway. Inhibitory neurons project only to inhibitory dendrites and excitatory neurons project only to excitatory dendrites. Each dendrite has an associated set of synaptic weight vectors, W_{fe}, W_{λ}, and W_{fi}, corresponding to the excitatory feeding field, linking field, and inhibitory feeding field pathways, respectively. Each weight vector also has an associated gain scalar, V_{fe}, V_{λ}, or V_{fi}. These scalars are strictly for convenience in altering the connection strengths in our simulation software. We globally raise or lower the excitability of a neuron by increasing or decreasing the gain scalars. The total synaptic weight is the product of the scalar and its associated weight.

The basic kernel is a "spike density modulator" or SDM (Eckhorn et al., 2004). It consists of a single layer of excitatory neurons with reciprocal linking field connections and an inhibitory neuron. The excitatory neurons all project to the inhibitory neuron and to targets outside the kernel. The inhibitory neuron feeds back to the inhibitory dendrites of all the excitatory neurons in the kernel (Eckhorn, 1999). The dynamics of the SDM are central to the ability of the network to synchronize incoming signals, to be frequency-selective, and to the ability of a chain of functional columns to propagate or suppress traveling waves. In addition, as we will show later, these dynamics are responsible for the production and propagation of pulse "packets" in the presence of non-synchronous input signals. This is an interesting feature for reasons we will discuss. We report several neurodynamic modes of operation found in our cell groups and assemblies. These dynamics are responsible for the signal generation and propagation characteristics we report and for production of subharmonic and anharmonic spectral components in the overall firing activity of the network. We conjecture that this may be one mechanism behind the presence of local alpha- and beta- frequencies in the cortex as characterized, e.g., by Bruns and Eckhorn (2003). Finally, the theory describing the key dynamical properties of an SDM is surprisingly simple, and this makes these networks easy to design and analyze.

2. Methods

2.1 Basic Dynamical Properties of the Excitatory Dendrite

Many of the important properties of our networks are determined by the parameters of the excitatory dendrites and the baseline firing threshold, θ_0, of the neuromime. We first consider the case where the neuron is receiving a synchronous volley of feeding field pulses over some set of excitatory synapses of the form

$$y(t) = \sum_{n=0}^{N} \delta(t - nT) \,. \qquad (1)$$

Each synaptic input signal $y_k(t)$ is frequency-locked with zero phase delay at a fundamental frequency given by $f = 1/T$. (In this paper we use the word "synchronous" to denote this condition; if signals are frequency-locked but have relative phase delays we call them "phase-locked"; signals that are not frequency-locked we call "asynchronous"). If each feeding field synapse has the same integration time constant τ_{fe} the output $x_{\text{fe}}(t)$ of the dendrite's feeding field pathway in the absence of linking field inputs is governed by

$$\tau_{\text{fe}} \frac{d\,x_{\text{fe}}(t)}{d\,t} = -x_{fe}(t) + \text{V}_{\text{fe}} \sum_k w_k y_k(t) \qquad (2)$$

where the w_k are synaptic weights, the summation is taken over the active inputs, and V_{fe} is the gain scalar mentioned earlier. We define the excitation factor μ as

$$\mu = \text{V}_{\text{fe}} \sum_k w_k \qquad (3)$$

and note that μ is a function of the number of active inputs and their associated weights.

The solution of (2) given inputs (1) at time $t = NT$ for an initial condition of zero is

$$x_{\text{fe}}(NT) = \mu \frac{1 - \exp\left[-(N+1)T/\tau_{\text{fe}}\right]}{1 - \exp\left[-T/\tau_{\text{fe}}\right]} \quad . \qquad (4)$$

There are two parameter-dependent classes of special cases we must consider. First, if the ratio of the excitation factor to the baseline threshold is such that $(\mu/\theta_0) \geq 1$ the neuron will fire at the first ($N = 0$) pulse input (spatial summation condition). For given values of T and μ it is always possible to select linking field parameters and the refractory parameters of the neuromime's variable threshold

$$\theta(t) = \theta_0 + V_s \exp\left[-\left(t - t_{spike}\right)/\tau_s\right] \qquad (5)$$

such that the neuron spikes only once in response to each input pulse. Here t_{spike} is the time the neuromime last fired. We call this the "all-pass follower" (APF) condition since the neuron simply repeats at its output the incoming signal. Contrariwise, a different selection of parameters for the neuromime and the linking field can be made such that the neuron outputs more than one spike in response to a single input volley. We call this the "burst" condition. We will not be concerned with the burst condition case in this paper.

The second class concerns those cases where $(\mu/\theta_0) < 1$. This is the class of frequency-selective SDMs (spatio-temporal integration). We first consider frequencies $f = 1/T$ for which

$$\lim_{N\to\infty} x_{fe}(NT) = \mu \frac{1}{1 - \exp\left[-T/\tau_{fe}\right]} < \theta_0 \,. \qquad (6)$$

In this band of frequencies an input tetanus lacks the ability to evoke a firing response in the absence of linking field enhancement of the excitation factor. We call this case the "high pass filter" (HPF) condition. The highest frequency $f_c = 1/T_c$ for which the HPF condition is met is called the stopband edge. The SDM will not propagate or respond to an input tetanus that meets the HPF condition, and so we call cell groups for which the input kernel meets the HPF condition for some range of frequencies a high pass filter (HPF). The stopband edge is given by

$$f_c = \frac{-1}{\tau_{fe} \ln\left(1 - \mu/\theta_0\right)} \,. \qquad (7)$$

For frequencies $f > f_c$ the integrator action of the feeding field pathway will eventually produce a pulse response to the tetanus. Let $t = MT$, $0 < M$, be the time at which an output spike is evoked. Note that the first M input pulses in the tetanus will not propagate through the neuron. We call this "integrator loss" (IL). Note also that a HPF will *always* have an integrator

loss of at least 1 pulse since the neuron cannot respond to a single pulse under the HPF condition. The lowest frequency $f_p = 1/T_p$ for which M has some specified value is called the M-passband edge. In the text we usually abbreviate this to simply "the passband edge." The transition band is the band of frequencies f such that $f_c < f < f_p$. The M-passband edge is defined by the condition

$$x_{\mathrm{fe}}(T_p) = \mu \frac{1 - \exp\left[-(M+1)T_p/\tau_{\mathrm{fe}}\right]}{1 - \exp\left[-T_p/\tau_{\mathrm{fe}}\right]} = \theta_0 \ . \qquad (8)$$

T_c, T_p and either M or τ_{fe} are design parameters for a kernel. Equations (6) and (8) along with the HPF condition constraint are the corresponding design relationships. There are numerous numerical techniques, e.g. linear programming, that can be used to solve the design equations. Our ENs are designed for $M = 1$, which sets their f_p well within 1 Hz of f_c. Our HPF INs are designed for $M = 2$, which sets their f_p from about 8 to 39 Hz above their f_c, depending on their τ_{fe}.

There are two special cases under this class that need to be considered. We call the first case the "linear HPF" (LHPF) case. It is characterized by a range of frequencies $f_p \le f \le f_m = 1/T_m$ for which the particular parameter settings of the linking field and the neuromime are such that one output spike is produced for each input spike volley coming at $t \ge MT$. In our designs we use the linking field to synchronize incoming synaptic signals that have small relative phase delays with respect to each other. For our parameters the effect of the linking field dies out within about 5 msec of the output spike time t_{spike}. Consequently the LHPF region of operation is primarily determined by the neuromime parameters, which we discuss this below.

The second special case is that for which $T < T_m$. In this case $x_{\mathrm{fe}}(t) > \theta_0$ re-triggers the neuromime before the arrival of the next volley in the group's external input tetanus. We call

this the rate multiplier (RM) condition and it is central to some of the more interesting neurodynamics we will examine later. The RM condition likewise depends on the parameter selection for the neuromime but the complete dynamic of the effect brings into play the full dynamics of the kernel and of the functional column as a whole. We therefore postpone its discussion until later and merely note for now that under the RM condition a chain of functional columns will up-convert lower-band input signals (e.g. beta-band) into higher-band signals (e.g. gamma-band or higher) and propagate them over long distances.

2.2 The Inhibitory Neuron

The inhibitory neuron (IN) has no linking field input and no inhibitory dendrite in our kernel. The dynamics of its excitatory dendrite are precisely the same as described previously, the difference between an IN and an excitatory neuron (EN) being merely parametric. The IN is inhibitory only because it sends its output to the feeding field input of an inhibitory dendrite.

The IN can be designed to operate in HPF mode (in which case it has its own f_c and f_p), or it can be designed to operate in APF mode. Most of the INs in our networks operate in HPF mode, although in one of our functional columns some operate in APF mode in one of the cell groups.

The principal role of the IN in the SDM is regulatory. It limits the maximum steady firing rate of the kernel by breaking its outputs into "packets" for output frequencies above the IN's f_p. One thing this does is prevent the cell group from exhibiting spontaneous high-frequency oscillations. Another is to "packet" signals arising from an asynchronous input tetanus. When the incoming signals with rates above f_c are not frequency-locked one by-product is the production of spurious output pulses from the excitatory neurons in the kernel. As the input signal pulses coalesce in time (a "beat" phenomenon caused by the multiple input frequencies)

the effect on the excitatory neurons is to produce a burst of output pulses. An IN operating in the HPF condition will fire and break up these spurious outputs into packets of pulses. As the resulting output signals propagate down a chain of functional columns the spurious pulses and eventually the packets themselves are eliminated by the integrator loss mechanism of a HPF chain (provided the chain is not operating in RM mode). We call this the "evanescent mode" of propagation. Typically a packeted signal does not propagate for more than a few links in the functional column chain. In this way asynchronous input firing activity is localized to the immediate vicinity of its input in the overall network and only a long synchronous or phase-locked tetanus is able to propagate for long distances in a simple high-pass chain-of-functional-columns network.

The IN also limits the upper passband frequency of its kernel for synchronous input signals. Although we call a kernel a HPF kernel, it does in fact have an upper frequency limit imposed by its IN. The reason we do not call it a bandpass filter (BPF) is because the effect of the IN is modulatory and non-linear. The IN breaks the output transmission up into packets of pulses that propagate in evanescent mode in a chain provided the downstream functional columns are not designed to operate in either APF or RM mode.

For EN firing rates above the f_c of the IN the length of the packet is determined by where the EN firing rate falls in the transition region between f_c and f_p. If $f \geq f_p$ the packet will be a dipulse ($M = 2$). In the transition region M increases as f approaches f_c from above. An IN operating in APF mode always allows the kernel to transmit only a single pulse from its excitatory neurons. The IN does not, however, control the spacing between packets in our networks. This is done by the EN's inhibitory dendrite.

2.3 The Inhibitory Dendrite

For an EN driven by synchronous inputs the steady-state peak output pulses from its excitatory feeding field integrator have amplitude

$$x_{pk} = \frac{\mu}{1 - \exp\left[-T/\tau_{\text{fe}}\right]}$$

where $T = 1/f$. Suppose the neuron receives an inhibitory pulse from its IN at $t = t_{spike}$. Let

$$t' = t - t_{spike} .$$

The output of the inhibitory feeding field integrator is then

$$x_{\text{fi}}(t') = \mu_i \; e^{-t'/\tau_{\text{fi}}}$$

where τ_{fi} is the time constant of the inhibitory dendrite's feeding field integrator. The peak signal reaching the neuromime is $x_{pk} - x_{\text{fi}}$. In our designs $\mu_i > \mu$, which means that the EN will be inhibited from further firing until $x_{pk} - x_{\text{fi}} = \theta_0$. The time t_b required to achieve this condition is the blanking interval for the kernel. It is straightforward to show that

$$t_b = -\tau_{\text{fi}} \ln\left(\frac{\mu/\mu_i}{1 - \exp\left(-T/\tau_{\text{fe}}\right)} - \frac{\theta_0}{\mu_i}\right) . \qquad (9)$$

The blanking effect is most pronounced for high input frequencies. The usual effect is to produce one or more missing pulses in the kernel's output stream.

One thing that is important to comment upon is that t_b is generally *not* the spacing between packets in the output of a cell group. This is because there are interactions among the kernels in the cell group and in our design a missing pulse in one kernel is usually accompanied by missing pulses in other kernels that project to this kernel. Consequently μ, which is a function of the total number of active inputs converging on the kernel, can be reduced by a factor of 2 or more due to cell group dynamics. This can produce a spacing between pulse packets at the

output that is considerably longer than a t_b calculated without taking into account the feedback pathways within a cell group. If the "μ modulation" is taken into account in (9) then t_b gives the lower bound on the packet spacing interval. This particular dynamic is important in the reciprocal connection between kernels L-V(1) and L-V(2) in our cell group.

The blanking interval and the pulse packet spacing it generally produces leads to cell group dynamics that contains a *subharmonic* of the input frequency. Thus gamma-band inputs can result in signals with beta-band or alpha-band spectral components, beta-band inputs can result in alpha-band subharmonics, etc. Furthermore, if the IN fires because asynchronous inputs to the kernel have produced high frequency outputs that are not harmonics of the input signals, the resultant blanking and packet-spacing formations will produce additional spectral components that can be lower than the input frequencies but are not subharmonics. We call these "anharmonic sub-frequencies" to distinguish them from subharmonics.

2.4 The Linking Field

The linking field is the unique element in the Eckhorn neuron which promotes synchronization of the output firing of the linked neurons in response to poorly synchronized inputs to the feeding field (Eckhorn et al., 1990). The linking field integrator follows the dynamics of (2) with appropriate substitution of parameter variables. For a synchronous volley of k linking field pulses, $y_k = \delta(t)$, the linking field response is

$$x_\lambda(t) = \mu_\lambda \; e^{-t/\tau_\lambda}$$

where μ_λ is the linking field excitation factor and τ_λ is the time constant of the linking field integrator. The output of the excitatory dendrite in the presence of linking field activity is

$$x_e(t) = x_{\mathrm{fe}}(t)\left[1 + x_\lambda(t)\right] . \qquad (10)$$

In our kernel each of the excitatory neurons is linked to the others within that kernel. We arrange the neurons in a "ring" so that each EN has two nearest neighbors and one remote neighbor. The synaptic weights of the nearest neighbors are twice as large as that of the remote neighbor. Only neurons within a kernel are linked; linking fields are not shared between kernels. No neuron feeds back to its own linking field.

The synaptic weights and gain scalar V_λ of the linking field are set so that any linking field input received by a neuron results in an x_e in (10) sufficient to put the neuron into APF mode for any feeding field input. τ_λ is small compared to the other time constants in the neuron, so the linking field inducement of APF mode persists only over a window of about 5 msec from the time of the linking field input. During this window the neuron is able to "capture" poorly synchronized incoming signals that would have otherwise not evoked a firing response. A more detailed description of the capture effect has been given by Johnson (1994).

In the simulations we present in this paper the external inputs applied to the input kernel of the network each connect to only one EN within that kernel, via the feeding field input, and so the effect of the linking field in the input kernel is to synchronize the output firing pattern of the input kernel in the presence of input pulses with relative phase delays of a few milliseconds. Mathematically, if one EN in the input kernel fires, the linking field effectively lowers f_p to zero for the other neurons in that kernel during the time window defined by x_λ in each neuron. One can regard the linking field signal as constituting a modulation of the feeding field excitation factor

$$\mu(t) = \left(\mathrm{V_{fe}} \sum_k w_k \right) \cdot \left(1 + \mu_\lambda \, e^{-(t - t_{spike})/\tau_\lambda} \right) \qquad (11)$$

where t_{spike} is the arrival time of the linking field input pulse.

2.5 The Neuromime

The neuromime consists of a discriminator ("comparator") and a threshold variation function (Eckhorn et al., 1990). Its input signal is $u(t) = x_e(t) - x_{fi}(t)$ where x_e is given by (10) and x_{fi} is the output of the inhibitory dendrite (if there is one). $u(t)$ is compared to a threshold $\theta(t)$. If $u(t_0) < \theta(t_0)$ the neuron output is $y(t) = 0$. Otherwise $y(t) = \delta(t - t_0)$ and $\theta(t)$ is re-set according to (5). We use a neuromime refractory time factor V_s that is much greater than the maximum μ of the excitatory dendrite even with maximum linking field modulation. This forces the neuron to have an absolute refractory period of at least 4 msec using our parameters.

There are two mechanisms by which the neuromime can act as a rate multiplier producing multiple output spikes in response to a single input volley. The first mechanism occurs when the threshold $\theta(t)$ falls below the residual output of the excitatory dendrite (assuming no inhibition influence by an inhibitory dendrite) in the absence of a new feeding field input pulse. Let x_0 be the state of the feeding field integrator at the time the neuromime emits a spike. We take this spiking time as our $t = 0$ reference. The neuromime will produce a second output spike if there exists a time $t > 0$ such that the ratio of $u(t)$ to $\theta(t)$ equals unity, i.e.

$$\frac{x_0 \cdot \exp(-t/\tau_{fe})}{\theta_0 + V_s \cdot \exp(-t/\tau_s)} \cdot (1 + \mu_\lambda \cdot \exp(-t/\tau_\lambda)) = 1 \ . \qquad (12)$$

Note that μ_λ can be zero in (12). With our parameters it can be as large as 12.5. If a $t > 0$ exists that satisfies this condition the neuromime will re-fire. This is operation in the mode of a bursting neuron. There are numerous ways to evaluate (12), the simplest being to merely graph the function and see if it exceeds unity. None of the neurons in our networks satisfy condition (12).

The second mechanism for producing RM mode operation is from internal feedback from

other neurons in the cell group. Our cell groups are recurrent neural networks and there are important signaling conditions in which this mechanism produces RM mode operation. We will see later that this dynamic has some very interesting results. Assume the neuron has fired at t = 0 and that at some time $t = \Delta T$ it receives an excitatory feedback volley with excitation factor μ_{net}. Condition (12) is then modified to

$$\frac{x_0 \cdot \exp(-t/\tau_{fe}) + \mu_{net} \cdot \exp(-(t-\Delta T)/\tau_{fe}) \cdot h(t-\Delta T)}{\theta_0 + V_s \cdot \exp(-t/\tau_s)} \cdot (1 + \mu_\lambda \cdot \exp(-t/\tau_\lambda)) = 1 \qquad (13)$$

where $h(t)$ is the Heaviside function. In most practical cases the linking field term is negligible since when it is active the neuron is also usually deep inside its refractory period. Because x_0 is generally greatest when the input signal bombardment is a high-frequency tetanus, the condition for (13) is usually met with only for input signals well above the f_c of the neuron. In our network model we incorporate a 1 msec synaptic delay for signal propagation through a neuron and so ΔT is easily determined for any feedback pathway.

2.6 The Cell Group

Figure 1 illustrates the structure and connectivity of the cell group. The group is comprised of six kernels of five neurons each (4 excitatory, 1 inhibitory) organized into "layers" along the general lines of the cortical organization reported by Douglas and Martin (2004). Our specific topology departs from the interaction graphs they reported; however, because of the synchronized firing patterns observed within the column, we believe our topology to have a mathematically equivalent input-output dynamic. Layer designations and reference numbers for the neurons are shown in the figure. The inhibitory neurons (INs) carry numbers that are multiples of five (5, 10, etc.). Consecutively numbered excitatory neurons (ENs) are contained within the same kernel. The kernel designators ("layer designations") in order of the neuron

numbers are: L-IV, L-III(1), L-III(2), L-V(1), L-V(2), and L-VI.

Figure 1

Projections from a kernel are by the excitatory neurons only. Each EN in the source kernel projects to every neuron in the destination kernel. Each destination neuron equally weights the synaptic strength of the connections from the source neurons; however, the weights for ENs in the destination kernel differ from those given to the IN. 95% of the Σw for an IN comes from the ENs within its own kernel. Thus the influence of projections coming into an IN from outside the kernel are slight but not negligible. A different kernel acting by itself cannot stimulate the firing of the IN but it can slightly bias it in the direction of firing (effectively, a decrease in the IN's f_c of about 4 Hz).

The decision to project to every neuron within the destination kernel was based on anatomical studies reported by White (1989A). White summarized his findings as basic rules governing the synaptic organization of the cerebral cortex, and we used "White's rules" as a guide in coming up with the cell group connectivity. We used equal-valued synaptic weighting of a source kernel's afferents because in the absence of an *a priori* reason to do otherwise it seemed best to us to design the cell group with an eye toward its future use in recurrent chain and array networks. In particular, we decided to set up the cell group to accord with Wang's "equal-sum-of-weights" condition (Wang, 1995). We use the same weight assignments for all cell group designs and employ V_{fe} and τ_{fe} to alter the kernel properties for cell groups tuned to different passbands. Our synaptic weight assignments are tabulated in the appendix.

Inputs to the group come into L-IV. In the simulations reported in this paper the first column in a chain has a single input to each excitatory neuron in L-IV, representing an "input tract." Each input tract is given a synaptic weight $w = 1$. All our cell groups are "high pass filter"

structures. The HPF function is implemented in L-IV, the input kernel, for a specified f_c and f_p. The HPF has a very steep transition band (M = 1), much less than 1 Hz wide, so L-IV will respond to any incoming tetanus with rate greater than f_c on the second received pulse. L-IV will not respond to a tetanus of inputs with rates less than f_c. The excitatory neurons in the other five kernels all operate in APF mode in the absence of inhibition when L-IV fires synchronously. In this paper we present three cell group designs, one beta-band HPF and two gamma-band HPFs.

2.7 The Bandpass Column

A cell group used as a functional column can only implement a HPF. To implement a bandpass filter (BPF) that will selectively respond to synchronous inputs within a specified upper and lower frequency we employ two cell groups, tuned to different frequencies, in a feedback arrangement. The BPF functional column is shown in figure 2.

figure 2: 2 columns wide

The input to the functional column is L-IV of cell group 1. This cell group implements the lower passband frequency and rejects inputs below this frequency. L-III(2) of group 1 projects excitatory signals (denoted by arrowheads) to L-IV of cell group 2. Group 2 is a HPF tuned to the desired high-frequency corner, beyond which the column will suppress synchronous signal transmission. The inhibitory neuron in group 2 L-III(2) projects back to the excitatory neurons in group 1 kernels L-V(1), L-V(2), and L-VI. Thus if group 1 responds to inputs above the f_c of group 2, group 2 begins firing and thereby inhibits group 1. Here we note that in our chains of functional columns we use L-VI of group 1 as the output port of the column. The inhibitory feedback from group 2 inhibits the kernels it targets buts allows L-IV, L-III(1), and L-III(2) of group 1 to continue to fire. This ensures that group 2 will continue to fire so long as group 1 is

receiving inputs above the desired high-frequency cut-off of the BPF. Figure 3 illustrates our chain of functional columns. In this paper we present results for a chain of HPF functional columns and a chain of BPF functional columns.

figure 3

3. Results

3.1 Chain of Gamma-Band High Pass Filters

Our first case is a chain of identical functional columns with each column consisting of a single cell group designed to act as a HPF for gamma-band frequencies (γ-HPF). L-IV is designed for f_c = 27.16 Hz. The parameters of this cell are provided in the appendix. There are four external inputs to column 1, each input terminating on a single EN in the kernel with synaptic weight w = 1. The four outputs of L-VI project to all four ENs in L-IV of column 2 with synaptic weight w = 0.25. L-IV has a μ/θ_0 ratio of 0.99937 with regard to external inputs, i.e. L-IV is at the edge of APF mode operation. The μ/θ_0 ratio for feedback inputs from L-VI to L-IV (see figure 1) is also 0.99937. Equation (13) verifies that L-IV can not operate in RM mode despite being balanced just below APF threshold. Likewise, none of the other kernels in the group operate in RM mode. Therefore the cell group is zero-input stable, i.e. it cannot spontaneously produce oscillations nor can it be triggered into producing self-sustaining oscillations.

All the inhibitory neurons in the cell group have an f_c = 53.4 Hz when stimulated by the ENs within their kernels and an f_c = 48.9 Hz when stimulated by all sources. The functional columns therefore have a passband to synchronous input signals running from $27.1 < f < 48.9$ Hz. Our simulations with synchronous inputs confirm this passband. Outputs from each column are

synchronized (by the linking field) with no relative phase delay in the output signals.

The propagation of signals down a chain in the passband is evanescent due to integrator loss. For instance, if the external input is a train of M phase-locked pulses, column 1 will pass M – 1 pulses, column 2 will pass M – 2 pulses, etc. Thus a finite-duration tetanus in the passband of M pulses will propagate down only M – 1 links in the chain. This is independent of the input frequency (so long as it is within the passband) and so the propagation *distance* is directly proportional to the length (in pulses) in the input tetanus. One can regard this as an interesting form of "spatial encoding" of input signal information.

3.1.1 Pull-in by Secondary Stimulation

By far the most interesting dynamics occur at the band edges and for asynchronous input signals relatively close to each other in frequency. The first example we will look at is a short-propagation-distance phenomenon we call "pull-in by secondary stimulation." We will examine an example of this in detail because, firstly, the neurodynamics are interesting and, secondly, because it illustrates the ability of the theory described earlier to *exactly* explain these dynamics.

Figure 4 illustrates the response of neurons N1-N15, i.e. layers L-IV, L-III(1), and L-III(2). Output layer L-VI precisely tracks L-III(2) with a lag of 1 msec. The input signals consisted of one 28.57 Hz (T = 35 msec) tetanus applied to N1 and three 27.03 Hz (T = 37 msec) signals (zero relative phase delay) applied to neurons N2-N4. N1 receives its first pulse at t = 34 msec; N2-N4 receive their first pulses at t = 36 msec.

figure 4

All four neurons "swallow" their first input pulse (integrator loss). At t = 69 msec N1 receives

its next input and, because the input rate is within its passband, it fires in response at t = 70. By itself N1 does not have sufficient strength to fire L-III(1) because this layer requires a minimum of two inputs from L-IV to operate in APF mode. It does, however, send a linking field pulse to N2-N4, which arrives at t = 71 msec. In the absence of this linking field pulse, N2-N4 would not fire when they receive their inputs at t = 73 msec because this rate is below their cutoff frequency f_c. However, with the linking field enhancement of their μ values their excitation factors are large enough (just barely) to fire in response to their inputs. (If the period of their input signal had been 39 msec instead of 37 msec they would not have responded). Their firing puts L-III(1) and the other kernels into APF mode and the column responds with its first output pulse at t = 77 msec.

When N2-N4 receive their third input pulse at t = 110 msec their feeding field integrators are still partially "charged" by the firing of L-VI at 77 msec (33 msec earlier); they now "see" an effective input frequency of 30.3 Hz and so their second firing would take place even in the absence of the linking field pulse from N1. Because this firing is stimulated by the earlier firing of L-VI, we call this "secondary stimulation." For the rest of the first packet of firing by N2-N4 until t = 296 msec, N2-N4 have a stable firing pattern stimulated by L-VI and synchronized to their external inputs with a period of 37 msec. Were it not for N1, which "kick started" this process via the linking field, this would continue as long as the inputs to N2-N4 lasted. This is what we mean by "pull-in by secondary stimulation."

Next we note the third and fourth output pulses from N1. They constitute a dipulse with a spacing of 9 msec between pulses. The first pulse (t = 140) is due to N1's external input. The second is due to stimulation by L-VI, which succeeds in re-firing N1 because N1's input pulse now leads the next input pulses to N2-N4 by a sufficient time to allow N1 to come out of its

refractory period (equation 13). N1 is now also in secondary stimulation, only in its case the result is a dipulse pair rather than a single output pulse. However, this is not RM mode operation because if the N2-N4 inputs were to cease then N2-N4 would stop firing and the N1 dipulses would cease also. N1 would simply respond to its input tetanus. Note that the column's firing pattern up to and including the pulses at t = 296 msec are in sync with N2-N4.

The secondary stimulation dynamic comes to an end with the arrival of N1's ninth input pulse at t = 314 msec. Here, for the first time since secondary stimulation set in, N1's input pulse *lags* the input pulses of N2-N4 by enough to allow N1 to re-fire L-III(1). Note how at this time L-III(1) and L-III(2) follow N1 instead of N2-N4. The output firing N1 now evokes causes N2-N4 to produce dipulses, the second of which occurs at t = 319 msec. This in turn finally stimulates inhibitory neuron N5. In addition, the combination of the linking fields from N2-N5 arriving at N1 coincidently with the firing by L-VI is sufficient to re-fire N1 as it is coming out of its refractory period (producing the high frequency dipulse seen at t = 320). Feedback from N5 to the inhibitory dendrites of N1-N4 (which have a time constant τ_{fi} = 15 msec) brings secondary stimulation to an end and produces the long gap between the first and second packets from t = 320 to t = 525 msec. At these input frequencies the effect of the inhibition prevents N1 from firing until t = 476 msec. Note that N2-N4 cannot re-fire until N1 starts firing again.

The first time N1 can respond after inhibition release is for its input at t = 489; however, N1's firing is now too far away from the last inputs to N2-N5 (t = 480 msec) for its linking field signal to trigger them. At its t = 524 input N1's linking field can stimulate N2-N5 and the process begins again with one difference. This time, owing to the relative phases of the input signals (a beat condition), it is N1's linking field signal that fires N2-N4. Their next input produces the second output pulse from the functional column at a dipulse spacing of 30 msec (t

= 526 and 556). Referring to figure 5(a), these two rapid pulses put column 2 into a secondary stimulation mode and, since the output pulses from column 1 quickly settle into a 37 msec pulse period, column 2 propagates a synchronized version of the N2-N4 input signal until column 1 comes out of its secondary stimulation mode. (The output dipulse from column 1 does not appear in figure 5(a) because the first of these two pulses is "swallowed" by integrator loss in column 2). Because the output of column 2 consists of four synchronized 27 Hz pulse trains, column 3 rejects the input, as shown in figure 5(b), and the dynamic propagates no farther. Column 3 does pass on the dipulse at approximately t = 950 msec, but column 4 "swallows" the first pulse (integrator loss) and column 5 "swallows" the second. Column 6 does not receive any of the upstream signals.

figures 5(a), 5(b)

Pull-in by secondary stimulation is an emergent property of this network, but the key point to this discussion is: the theory discussed earlier perfectly describes every aspect of this interesting non-linear dynamic. If one thinks to look for the phenomenon *a priori*, the theory would predict it.

3.1.2 Packeting

Another interesting dynamic observed when all the input signals are in the passband is packeting. The packeting effect is particularly dramatic when there are enough phase-locked inputs to ensure that their corresponding L-IV neurons can cooperatively fire L-III(1) in APF mode. Figure 6 illustrates the response of column 1 kernels L-IV, L-III(1), and L-III(2); the output follows L-III(2). The column is driven by two inputs with T = 22 msec (N1-N2) and two inputs with T = 21 msec (N3-N4). There are three packets clearly visible in this plot. It is also clear that within each packet the outputs of L-III(2) (neurons N11-N14) are phase-locked. The

first packet has a period of 21 msec. It is also observed that each packet terminates with a higher-rate dipulse that evokes firing by the inhibitory neurons N5, N10, and N15.

figure 6

This is not a linking field phenomenon and, indeed, the linking field has nothing to do with the dynamics seen in the figure. What happens is this. The second volley into N3-N4 at $t = 41$, arriving before the volley into N1-N2, fires these neurons, and these in turn fire L-III(1) in APF mode. This causes the firing of the rest of the kernels. L-VI, feeding back to L-IV after a 3 msec delay, would have fired N1-N2 even in the absence of their next external inputs. As it is, these inputs arrive 2 msec before the L-VI feedback; the later-arriving volley is simply lost in the refractory period of N1-N2. But by the fourth N3-N4 output volley at $t = 105$ the feedback from L-VI arrives before the N1-N2 input volley and fires N1-N2 at $t = 109$. This is *phase-locking through L-VI feedback*. L-VI continues to determine the firing of N1-N2 for their next 7 pulses.

As time goes on, the input signals for N1-N2 lag those of N3-N4 by a greater and greater amount until finally, at $t = 263$ msec, they lag enough to re-trigger N1-N2 as they come out of their refractory period after firing in response to L-VI. This produces the characteristic dipulses (dipulse spacings = 11 and 13 msec) that terminate the packet by firing the inhibitory neurons.

The time constant of the inhibitory dendrite combined with the periods of the input signals determines the width of the spacing between adjacent packets. Inspection of the second packet shows that N1-N2 initially lead N3-N4; this is due to the on-going time-shift between the two tracts of external driving signals. Since N1-N2 can also drive L-III(1) in APF mode, at the start of the second packet they control the firing interval of the L-VI output (22 msec) and its firing time. However, N3-N4 slowly re-take the lead in arrival time and control of the packet turns

over to them. By $t = 486$ an L-VI firing interval of 21 msec is re-established.

The key to this dynamic is to have a sufficient number of in-band phase-locked afferents such that their target neurons in L-IV can fire L-III(1) in APF mode. In the example we have just seen, both input tracts satisfy this condition, and which controls the output firing rate switches back and forth as the input firing times drift past each other. The packet dynamics become considerably richer if there is only a single "dominant tract" that satisfies the condition of firing L-III(1) in APF mode (e.g. $T_1 \neq T_2 \neq T_3 = T_4 \neq T_1$). In this case many more packets can form for brief intervals, interspersed with occasional longer ones when the dominant tract neurons (e.g. N3-N4) get the lead in firing L-VI. But generally neither the packet width nor the spacing between packets settles to a uniform value; however, a packet always terminates with a dipulse.

Packet propagation is evanescent. Each succeeding link in the chain will drop the first arriving input pulse from integrator loss and the packet is chewed up pulse-by-pulse as it propagates down the chain.

3.2 Chain of Beta-Band Bandpass Filters

Next we consider a BPF chain network with functional columns as shown in figure 2. The cell group parameters are given in the appendix. The functional column is designed to be a beta-band BPF with a passband for synchronous inputs from 15 Hz to 25 Hz. The lower passband edge at 15 Hz was achieved by modifying L-IV of the beta cell group (group 1). L-IV is given a τ_{fe} of 15 msec and θ_0 is raised to 0.606; otherwise the parameters for L-IV's excitatory neurons are the same as were used in the γ-HPF described above. Excitatory neuron parameters for the other kernels in group 1 are the same as previously. The inhibitory neurons for group 1 were made slightly less excitable; specific parameters are given in the appendix. Group 2 (the gamma-band HPF) is essentially the same as previously described except for the inhibitory

neurons in the kernels other than L-IV. These neurons were made more excitable such that they operate in APF mode for inputs from the excitatory neurons in their kernels.

The most important new dynamic introduced by this network is operation in RM mode by kernel L-IV of group 1. As we will show, this dynamic makes it possible for this network to have true traveling wave propagation; more interesting still, this propagation is by dipulses *at frequencies well above the beta-band* (and in this sense our name "β-BPF" is a bit misleading). Furthermore, these high-frequency dipulses are produced by group 1, i.e. group 1 *generates* the supra-beta-band waves it propagates. In all particulars the RM mode operation of the functional column is precisely predicted and explained by the theory presented earlier. We will also demonstrate that this network generates subharmonics in the alpha-band and in the low-frequency band as well.

We begin with the rather ordinary details of operation in response to synchronous inputs in the β-passband. Like the earlier HPF, the functional column merely passes these signals along. Group 2 remains inactive and the propagation is evanescent, i.e. each link in the chain "swallows" the first pulse it receives via the IL mechanism. The column rejects inputs below its f_c (14.4 Hz for the parameters reported here).

The concept of "upper passband edge" becomes rather interesting for this structure. For synchronous inputs of 27 Hz or higher there is no propagation beyond link 2 in the chain. This is because the γ-HPF becomes active in the first link and limits the output of this link to a pair of pulses. After this the inhibitory feedback into group 1 suppresses any further firing action by L-VI of group 1. The output pulses are subject to integrator loss in the next links and so the evanescent travel distance is effectively limited to a single pulse arriving at the third link. The one pair of pulses link 1 does generate are packeted by the induction of RM mode in L-IV.

Figure 7 illustrates the dynamic. We observe for N1-N4 the generation of two normal firing responses, the second occurring at just past t = 100 msec, followed by an extra firing event. This pulse is due to L-VI re-triggering the neuromimes in N1-N4 prior to the arrival of the next input pulses. Two output pulses are generated by L-VI (N26-N29). The RM dynamic requires L-VI to generate *both* output pulses. The first output pulse (t < 100) acting alone cannot re-trigger L-IV. The RM mode induction requires three external input volleys to "charge up" the feeding field integrators of N1-N4 before L-VI can re-trigger L-IV.

figure 7; two columns wide

Figure 8 illustrates the firing patterns in the γ-HPF by L-IV, L-III(1), and L-III(2). The inhibitory neuron (N45) in L-III(2) feeding back to group 1 inhibits further firing of group 1's L-VI, as is seen in figure 7. The firing dynamic in group 2 L-III(2) is also interesting. Note that this kernel is firing at one-half the rate of L-III(1). Kernels L-V(1), L-V(2), and L-VI behave similarly. Volleys into L-III(2) from L-III(1) are not strong enough to overcome the effect of the previous firing of L-III(2)'s inhibitory neuron at the time of the "missing pulses" in the L-III(2) output tetanus. However, the synaptic weights linking L-IV to L-III(1) are three times larger than the weights linking L-III(1) to L-III(2), L-V(1), and L-V(2). Consequently L-IV is able to overcome the inhibition and re-fire L-III(1), but L-III(1) cannot pass this signal along to the subsequent kernels.

figure 8

Column 2, the next link in the chain, swallows its first input pulse (integrator loss) and responds to the second. However, no RM mode is induced in its L-IV because, as stated above, its L-VI must fire twice to induce the mode. Because there is no third pulse received, RM mode induction does not occur in column 2. It outputs a single pulse to column 3, which swallows

this pulse and brings an end to further propagation.

3.2.1 Traveling Wave Generation by RM Mode

The dynamics just described are all evanescent propagations. The situation changes dramatically when the network receives either asynchronous inputs in the beta-band or phase-locked beta-band inputs having sufficient relative phase delay. (Recall that we employ the word 'synchronous' to mean frequency-locked with zero phase delay, i.e. perfect synchronization). In these cases the network responds in RM mode and generates traveling waves in the form of pairs of pulses (dipulses). For phase-locked inputs, "sufficient" phase delay is a function of the input frequency; generally, lower frequency signals require larger relative phase delays to induce RM mode. If less than a "sufficient" phase delay is present the result is the same as for synchronous inputs, i.e. evanescent propagation of the input in non-RM mode. We have not yet worked out a closed-form expression of a sufficient condition for phase delay in phase-locked inputs to induce RM mode.

We illustrate this dynamic for asynchronous inputs of periods 52, 50, 47, and 45 msec (19, 20, 21, and 22 Hz), i.e. mid-beta-band, applied to N1-N4 of column 1's β-HPF. We chose this case because the signal dynamics in column 1 look quite involved yet the wave that is propagated is surprisingly simple-looking. Other examples differ in numerical details but not in fundamental mechanisms nor in the main results we illustrate here.

Figure 9 shows the firing dynamics of column 1/group 1. The initial dynamics are illustrative of the response of the network to asynchronous inputs. N4 receives its second input pulse and responds by firing at $t = 90$. N3 receives its second input pulse and fires at $t = 94$. Coming this soon after the firing of N4 this is sufficient to fire L-III(1), leading to the firing of L-VI at $t = 97$. L-VI fires N1-N2 at $t = 98$ (pull-in) and re-stimulates N3-N4 into firing at $t = 99$ (RM re-

triggering). This is evident in the figure from looking at the first two firings of N3. The feeding field integrators in L-III(1) are sufficiently "charged" by this firing sequence to re-trigger firing in L-III(1) as soon as their neuromimes come out of their refractory period at t = 104 (APF mode firing).

figure 9; two columns wide

This re-stimulated firing of L-III(1) is not sufficient to re-fire L-III(2), L-V(1), or L-V(2) within their refractory periods because the coupling weights from L-III(1) to these other kernels are only one-third that of the coupling weights from L-IV to L-III(1). Although V_{fe} for these kernels is same as for L-III(1), the μ value is smaller and therefore their relative refractory period is longer than that of L-III(1). Thus the effect of re-firing of L-III(1) never reaches L-VI.

At t = 103 N1 receives its second external input pulse. At the time of arrival N1 is well within its refractory period due to the pull-in firing at t = 98, and so its response to this input pulse is delayed until it comes out of the refractory period and fires at t = 110. It sends a linking field pulse to N2-N4 and this pulls-in these neurons, which re-fire at t = 111 (linking field synchronization). This again re-stimulates L-III(1), and this time its firing can propagate through the downstream kernels and generate firing at L-VI. However, the three rapid firings of L-III(1) now also stimulate its inhibitory neuron N10, which locks out further firing by L-III(1). This is evident in figure 9 from the spacing between the bursts of L-III(1) firing. L-VI fires for its second time at t = 114 (3 msec after the last firing of L-IV) and this re-triggers L-IV into firing in RM mode in N1 at t = 122 and N2-4 at t = 123. The inhibition of L-III(1) prevents this from propagating into the network, and L-IV's inhibitory neuron N5 now fires, preventing further re-stimulation of L-IV by the next volley of input pulses.

We have taken this detailed look at the firing dynamics in order to bring out the key

interactions taking place. One of them is the role of the interaction between μ and the parameters of the neuromime (θ_0, V_s, and τ_s) in setting an upper limit of the firing rate of the kernels in the network. Also central to this dynamic is the propagation time through the kernels (1 msec in our networks) and the stabilizing role of the inhibitory neurons. Third, the action of the linking field in synchronizing kernel firing is clear. We need not repeat these details for the rest of the column 1/group 1 firing activities shown in figure 9. The dynamics are complicated but the theoretical analysis of them is not.

Referring back to where we left off above, L-VI has now fired twice, producing a dipulse with dipulse spacing Δt = 17 msec. This is well above the f_c of the group 2 γ-HPF, and so group 2 fires *en mass* in response. The inhibitory neurons in group 2 are more highly excitable than those of group 1, and so this mass firing fires the inhibitory neurons in all group 2 kernels except L-IV. Inhibitory neuron N45 projects back to group 1 and places L-V(1), L-V(2), and L-VI of group 1 under an inhibition that lasts until just after t = 200 msec (see figure 9).

Let us now pass on to the dynamics of the downstream columns. Column 2 receives the transmitted dipulses, which we note are all *synchronized*, at the L-IV input of its group 1. Figure 10 illustrates the dynamics of column 2/group 1. L-IV swallows the first pulse in the dipulse (normal integrator loss) and responds to the second at t = 115. This stimulates firing of the entire group, leading to an output volley from L-VI (N86-N89) at t = 118. Feedback from L-VI to L-IV stimulates re-firing in RM mode. N61-N64 fire at t = 126, i.e. as soon as the neuromime threshold has decayed enough to permit re-triggering. This stimulates a second firing by the cell group, producing a second output at L-VI at t = 129. L-IV again undergoes RM re-triggering, producing a third pulse at t = 137. This results in a tri-pulse (inter-pulse spacings of 11 msec) being transmitted to group 2, which fires *en mass* at the second pulse in

the tri-pulse and projects inhibitory feedback from N105 to group 1 kernels L-V(1), L-V(20, and L-VI. The third pulse in the tri-pulse also fires the inhibitory neurons of L-IV, L-III(1), and L-III(2) in group 1 (N65, N70, and N75), bringing this firing epoch to a close. We note that group 2 inhibitory neuron N105 (in L-III(2) of group 2) fires at $t = 132$, i.e. *before* group 1 L-VI has a chance to respond to the third pulse in L-IV's tri-pulse. Thus the output of column 2 is limited to a single dipulse with a spacing of 11 msec.

figure 10; two columns wide

Much the same dynamic is repeated down the rest of the chain of columns. There is a slight decrease in dipulse spacing at column 3 (dipulse spacing 10 msec) because the column 2 dipulse spacing is only 11 msec instead of the 17 msec from column 1. However, the dipulse spacing from column 3 onward stabilizes at 10 msec due to the refractory period of the L-VI neurons in groups 1. Hence the minimum dipulse spacing is determined by the neuromime parameters, τ_{fe}, and μ in the L-VI kernel. The dipulse propagates as a traveling wave (saltatory propagation) along the chain of β-BPF columns regardless of the length of this chain.

The Fourier spectrum produced by the chain is interesting. We summed the neuron outputs from all neurons in a chain of three β-BPF columns, corresponding to the example just given, and calculated the magnitude of the Fourier transform of the resulting signal. This is meant to represent what one might obtain from an ideal probe covering the area occupied by these neurons (no frequency-dependent spacing loss due to physical separation of the probe from the neurons). The result is shown in figure 11. The frequency axis is in Hz and the magnitude axis is in "amplitude units" (a merely relative unit with no important physical significance to be attributed to the absolute value).

figure 11

The first interesting feature of this spectrum is the presence of subharmonics in the alpha band and in the sub-alpha band. One can easily make out spectral components at 3, 7, and 10 Hz, which are subharmonic to the 20 Hz and 21 Hz input signal components. There is also an anharmonic term at about 12.8 Hz. Although some contribution is made to the sub-beta-band region by packeting, most of the energy at these frequencies arises from the γ-HPF groups.

The next thing we note is the relative absence of energy in the beta-band. The input signals themselves are not included in the spectrum calculation, and so we conclude that the network generated very little, but not zero, energy in the beta-band. It produces significantly more energy in the gamma-band, and this is primarily contributed by group 1 of column 1, i.e. the *beta* network. Finally, we see a few significant peaks in the spectrum above the gamma-band. These are due to the dipulses and tri-pulses generated in RM mode. We close by remarking that the subharmonic and other characteristics of this spectrum seem to be fairly typical of these networks and not merely an artifact of the particular example from which figure 11 is generated.

4. Discussion

These are simple networks combining the desirable features of apparently complex neurodynamics with a surprisingly simple exact theory for analyzing them. We regard it as inconvenient that we have not yet been able to obtain an equally simple theoretical expression for the conditions under which phase-locked inputs to the BPF column pass over from synchronous propagation in evanescent mode to operation in RM mode. Having one would be more useful than an empirical characterization, e.g. by means of statistical regression. However, perhaps it is only a matter of time until such an expression is obtained.

In this paper when we have referred to the network's input signals we have invariably

assumed that all these inputs (four in the cases of our simulations) are firing. Furthermore, in order to simplify the analysis of the asynchronous input cases each external input coming into column 1 is projected to a single neuron in kernel L-IV with a synaptic weight $w = 1$. This gives the neuron a well-defined f_c and for synchronous input cases the f_c of the kernel is equivalent to the f_c of the individual excitatory neurons. For asynchronous inputs the kernel has no definably unique f_c.

In the context of a larger network in which our columns are embedded, this 1:1 input arrangement is in violation of White's rules. It is more biologically realistic in this case to distribute the input signals across $K \leq 4$ neurons in L-IV, giving each projection a synaptic weight w equal to one divided by the fan-in of the neuron (following the spirit of Wang's equal-sum-of-weights rule). For synchronous inputs this leaves the f_c of the neurons unchanged and the kernel still has the f_c of the individual neurons. In the case of asynchronous inputs, however, the L-IV neurons no longer have an f_c independent of the input signals and, likewise, the kernel has no definably unique f_c.

In considering the distributed-inputs case it is important to recall that μ is a function of the number of weights for *active* inputs. From (7) it is easily seen that as the number of active inputs goes down the f_c of L-IV increases. For our four-input networks, if L-IV has a stopband edge f_c for four synchronous inputs, it will have a stopband edge on the order of $6.7 \cdot f_c$ if only two inputs are active and synchronous (using our numbers for the β-HPF group). This quantizing-of-f_c effect decreases as the number of inputs in an input tract increases. For example, with 10 inputs under Wang's rule, if only 9 are active the stopband edge only increases to about $2.1 \cdot f_c$ using the same parameter values as before. However, because the logarithm is a very slow function there is a definite "diminishing returns" factor to consider.

For 25 inputs establishing f_c, having only 24 active still increases the response frequency to $1.5 \cdot f_c$. Put another way, the HPF L-IV kernel is *highly selective* in its spatial summation with regard to kernel f_c.

To model a cell group having a receptive field that takes in many inputs, not all of which are necessarily co-active, the network connectivity parameters should be made using μ as the design parameter for defining when a particular tract of *K* inputs within a larger network "goes active." One application of this consideration would come into play if one wishes to simulate a Hebbian-like learning environment with some adaptation rule, e.g. BCH (Bienenstock et al., 1982), to theoretically study the formation of hypercolumns. To a first approximation, valid when the synaptic weights *w* are all equal, μ is proportional to the number of inputs that define a synchronous tract. We make the conjecture that a Hebbian-like rule, e.g. the BCH rule, should probably be approached under the constraint of keeping the neuron's total $\sum w$ constant (Wang's rule again) and co-modifying V_{fe} to maintain μ for the tract being strengthened. This maintains f_c for the strengthened tract while increasing it for the tracts being weakened. We observe that because the other kernels in the cell group operate in APF mode to the synchronous firings from their sources, it does not appear useful (nor do we think it advisable) to adapt the internal synaptic weights of the cell group.

We find it especially interesting that these columns, particularly the BPF column, produce such a rich Fourier spectrum. It is well documented, e.g. (Bruns and Eckhorn, 2003), that the observable spectrum of activity in neocortex has a rich mixture of low-frequency, alpha-, beta-, and gamma-band components. The gamma-band has been much studied, and it is well known that cross-correlation coefficients for this and the other bands are generally fairly low in comparison with other fields of science. Many papers approach this sort of study with a tacit

assumption that one should look at the cross-correlation question as being one of correlating arriving signals at one location with transmitted signals from another. Our neurodynamics suggest that local self-generation of spectral components may be more important than is usually mentioned in the literature. The BPF column preferentially transmits traveling waves (in the form of dipulses) at frequencies higher than those of the incoming signals. To us this suggests it is not implausible that signal transmission in cortex may not be a simple matter of a signal being relayed from one location to another (although we think that some of this surely does take place). Rather, we think that local signal generation with non-linear frequency changing might play a more important role than we usually find discussed in the literature.

As the reader has no doubt noticed, the most biologically-unrealistic feature of the examples we have presented is the very rapid firing dynamics (particularly the RM mode dynamics) of which the cell groups are capable in a variety of situations. Neocortical pyramidal cell neurons in particular seem to lack the ability to fire at such high rates. Here we offer two comments. First, it seems to us quite clear that a proper adjustment of delays through the kernels and selection of neuromime values (particularly V_s and τ_s) can probably bring the maximum firing rates of the kernels into better agreement with accepted physiological values. We have not yet, however, attempted to do this and so this comment is a conjecture. Second, if the Eckhorn neurons each represent an assembly of even smaller groups of cells ("netlets"), it is not implausible that such a *netlet* might be capable of producing firing outputs (along different axons from different neurons at different times) that, taken collectively, would not be inconsistent with the model behavior reported here. We would be especially happy if our colleagues in neurophysiology and neuroanatomy were to deem it proper to take up this question.

Although the β-BPF does not propagate phase-locked signals in the gamma band, the same is not true for asynchronous gamma-band inputs. We have other simulations (not included here) demonstrating that RM mode operation of the β-BPF can generate and pass on dipulse packets, often with a fairly wide separation in time on the order of 100 msec or more, in response to such inputs. Our name "bandpass filter" should therefore not be taken too literally. The Fourier spectrum for these cases typically shows all the same features as presented above (generation of low- and alpha-band subharmonics, translation of frequencies into higher frequency ranges), but in cases of gamma-band asynchronous inputs we also observe significant spectral content in the gamma-band (albeit at different frequencies than the input signals) and we have also observed production of anharmonic beta-band spectral components. The dipulse outputs from L-VI are, of course, synchronous.

One thing the β-BPF will not do in response to these gamma-band inputs is generate a long tetanus of high-rate (that is, gamma-band) outputs from L-VI. This is made quite clear by the theory. However, this does not mean it is not possible to generate such a tetanus using the cell groups described here. For example, feedback from the output of a downstream column to column 3 can be made to stimulate re-firing of a train of dipulses by an appropriate selection of feedback delay, feedback weights, and neuromime parameters V_s and τ_s.

Left at this, such recurrently connected columns would oscillate until some other signal inhibited them. Recalling that f_c is determined by (7) and the width of the transition band by (8), another γ-HPF group can be added to one of the columns in the same way as is done in figure 2. This new group can be designed to integrate the output of its group 1 and fire at some time T_f after commencement of the oscillation. Inhibitory feedback from this "timing group" can then be used to set the duration of the tetanus.

An additional remark is in order concerning longer-distance cortico-cortical connections in a larger network. In this paper we have set up our chains to mimic signal transmission along adjacent columns. In other words, we regard column 2 in a chain as physically adjacent to column 1, column 3 to column 2, etc. Because pyramidal cells in layer 6 do project to layer 4 with a large-diameter axon arborization (Douglas and Martin, 2004) it seems at least plausible to use L-VI as the output port for projecting to the next link in the chain. However, if one were to model longer distance cortico-cortical transmissions, it is more faithful to current biological models to use the group 1 L-III(2) kernel as the projection port. As is easily seen from the simulation figures for the BPF columns, L-III(2) does maintain packeted, synchronous, and on-going gamma-band firing in column 1 in response to asynchronous inputs.

Other schemes are also no doubt possible using the basic cell groups as building blocks; this is what we like to call a "network of networks" approach to complex neural network systems, which is actually an old idea known rather poetically under another name as the "society of mind" concept (Minsky and Papert, 1988). Indeed, it was with this "network of networks" idea in mind that we came up with our cell group in the first place. Here again the possession of a simple theory for designing these networks is of great value. A colleague here at our Institute has commented to one of us that the dynamics of our networks appear to fall within the scope of the long-established theory of asynchronous state machines, a field in which he has expertise. We think this is a very interesting observation in light of the fact that the modern digital computer can be seen as nothing else than a neural network composed of McCulloch-Pitts neurons. Perhaps it might be that the world of computer engineering has something to offer computational neuroscience besides the computers with which we run our simulations.

The "network of networks" idea brings us to another point that has perhaps not escaped the

eye of the reader. Because the inner kernels in a group fire synchronously in APF mode, the four excitatory neurons in any of these kernels act effectively as if they were one neuron. It immediately follows from this observation that our cell group has "redundant" neurons and that some computational savings could be effected by replacing them with a single "effective neuron" in these kernels. We have not done so for two reasons. First, simulation of one second's worth of inputs for a network of 180 neurons only requires about 45 seconds of simulation time in MATLAB® on our machines. This is not much of a computational burden, nor do the "redundant" neurons complicate analysis in the least. Second, and more importantly, in a larger network-of-networks system in which one wishes to maintain some fidelity to the anatomical findings of neocortex research, one cannot rule out the need in future work to make non-APF projections into kernels other than L-IV. L-III(1), L-III(2), and L-VI immediately come to mind here. Therefore we allowed the "redundant" neurons to remain under the rule of thumb that it is easier to take things out later than it is to put them in later.

We remarked earlier that the evanescent propagation of a chain of HPF groups might be regarded as a form of spatial encoding: The distance a signal propagates downstream tells us something about the signal that originated it. Here we note that it is trivial to turn this evanescent propagation into true traveling wave propagation. Recall that in the HPF examples we have reported here the (μ/θ_0) ratio was set to just below unity in L-IV. This means that the HPF is balanced just at the edge of APF mode operation; a single additional input signal, arriving synchronously or with a small phase delay relative to the evanescent wave signal, is enough to push L-IV over into APF mode. This immediately suggests that a cross-coupled pair of parallel HPF chains, arranged in the manner of a synfire chain (Abeles et al., 2004; Hayon et al., 2005), will turn evanescent propagation into traveling wave propagation by the mechanism

of APF mode induction (which eliminates integrator loss).

To conclude, we have presented new neural network structures building on the Eckhorn neuron model (Eckhorn et al., 1990) and the pioneering networks based on them (Eckhorn, 1999). There is a simple theory both for designing and analyzing the dynamics of these networks. The basic cell groups arranged in chains of functional columns exhibit very interesting neurodynamics for signal propagation and generation. We have described in detail several interesting modes of operation in these cell groups. More complex neural networks can be constructed using these basic cell groups (with appropriate parameter design) by a "network of networks" approach.

5. Acknowledgements

This work was supported by the Idaho NSF-EPSCoR Program and by the National Science Foundation under award numbers EPS-0132626 and 0243885.

6. References

Abeles M, Hayon G, Lehmann, D (2004) Modeling compositionality by dynamic binding of synfire chains, J. Computat. Neurosci. 17: 179-201.

Anderson J, Lampl I, Reichova I, Carandini M, and Ferster D (2000) Stimulus dependence of two-state fluctuations of membrane potential in cat visual cortex, Nature Neurosci. 3: 617-621.

Bienenstock EL, Cooper LN, and Munroe PW (1982) Theory of the development of neuron selectivity: orientation specificity and binocular interaction in visual cortex, J. Neurosci. 2: 32-48.

Bressloff PC (1999) Synaptically generated wave patterns in excitable neural media, Phys. Rev. Lett. 82: 2979-2982.

Bruns A and Eckhorn R (2003) Task-related coupling from high- to low-frequency signals among visual cortical areas in human subdural recordings, Intl. J. Psychophysiol. 51: 97-116.

Campbell SR, Wang DL, Jayaprakash C (1999) Synchrony and desynchrony in integrate-and-fire neurons, Neural Computat. 7: 1595-1619.

Campbell SR, Wang DL, Jayaprakash C (2004) Synchronization rates in classes of relaxation oscillators, IEEE Trans. Neural Networks 15: 1027-1038.

Douglas, RJ and Martin, KAC (2004) Neuronal circuits of the neocortex, Annu. Rev. Neurosci. 27: 419-451.

Eckhorn, R (1999) Neural mechanisms of visual feature binding investigated with microelectrodes and models, Visual Cognition 6 (3/4): 231-265.

Eckhorn R, Reitboeck HJ, Arndt M, and Dicke P (1990) Feature linking via synchronization among distributed assemblies: Simulations of results from cat visual cortex, Neural Computat. 2: 293-307.

Eckhorn R, Gail AM, Bruns, A, Gabriel A, Al-Shaikhli B, and Saam M (2004) Different types of signal coupling in the visual cortex related to neural mechanisms of associative processing and perception, IEEE Trans. Neural Networks 15: 1039-1052.

Ermentrout GB (1998) The analysis of synaptically generated traveling waves, J. Computat. Neurosci. 5: 191-208.

Ermentrout GB and Kopell N (1986) Parabolic bursting in an excitable system coupled with a slow oscillation, SIAM J. Appl. Math. 46: 215-237.

Gibson JR and Connors BW (2003) Neocortex: Chemical and electrical synapses. In MA Arbib, ed. The Handbook of Brain Theory and Neural Networks, 2nd ed. The MIT Press, Cambridge, MA. pp. 725-729.

Hayon G, Abeles M, Lehmann D (2005) A model for representing the dynamics of a system of synfire chains, J. Computat. Neurosci. 18: 41-53.

Johnson JL (1994) Pulse-coded neural networks: Translation, rotation, scale, distortion, and intensity signal invariance for images, Applied Optics 33: 6239-6253.

Johnson JL and Ritter D (1993) Observation of periodic waves in a pulse-coupled neural network, Optics Letters 18: 1253-1255.

Kuramoto Y (1987) Statistical macrodynamics of large dynamical systems: Case of a phase transition in oscillator communities, J. Stat. Phys. 49: 569-605.

Medvedev G and Kopell N (2001) Synchronization and transient dynamics in chains of Fitzhugh-Nagumo oscillators using strong electrical coupling, SIAM J. Appl. Math. 61: 1762-1801.

Minsky M and Papert A (1988) Perceptrons (expanded edition), The MIT Press, Cambridge MA. pp. 266-268.

Osan R, Rubin J, and Ermentrout GB (2002) Regular traveling waves in a one-dimensional network of theta neurons, SIAM J. Appl. Math. 62: 1197-1221.

Rinzel JD, Terman D, Wang X-J, and Ermentrout GB (1998) Propagating activity patterns in large-scale inhibitory neuronal networks, Science 279: 1351-1355.

Rulkov NF, Timofeev, I, and Bazhenov M (2004) Oscillations in large-scale cortical networks: Map-based model, J. Computat. Neurosci. 17: 203-223.

Schuster HG and Wagner P (1990) A model of neuronal oscillations in the visual cortex: 2. Phase descriptions and feature dependent synchronization, Biol. Cybern. 64: 77-82.

Terman D, Ermentrout GB, and Yew AC (2001) Propagating activity patterns in thalamic neuronal networks, SIAM J. Appl. Math. 61: 1578-1604.

Terman D and Wang DL (1995) Global competition and local cooperation in a network of neural oscillators, Physica D 81: 148-176.

Wang DL (1995) Emergent synchrony in locally coupled neural oscillators, IEEE Trans. Neural Networks 6: 941-948.

White EL (1989A) Cortical Circuits: Synaptic Organization of the Cerebral Cortex Structure, Function, and Theory, Birkhäuser, Boston, MA. pp. 82, 157-158.

White EL (1989B) Cortical Circuits: Synaptic Organization of the Cerebral Cortex Structure, Function, and Theory, Birkhäuser, Boston, MA. pp. 58-62.

Figure Legends

Figure 1. The basic cell group. The cell group consists of 30 Eckhorn neurons arranged in kernels of five neurons each. The kernels are designated as L-III(1), L-III(2), L-IV, L-V(1), L-V(2), and L-VI. Each kernel contains four excitatory neurons and one inhibitory neuron. Projections between kernels are made by the excitatory neurons only. The cell group is called a highpass filter structure.

Figure 2. Bandpass Filter functional column. The column consists of two interconnected cell groups. Cell group 1 is the input group and is tuned to have the lower passband frequency. Cell group 2 is tuned to have the higher passband frequency. Both groups function as Highpass Filters. Column inputs come into L-IV of group 1. Inhibitory neuron N45 projects back to the group 1 neurons in L-V(1), L-V(2), and L-VI. Excitatory neurons in column 1 L-III(2) project to the external inputs of column 2 L-IV.

Figure 3. Connection of adjacent functional columns in a feedforward chain. In this arrangement we regard the columns as mimicking adjacent areas of cortex. Fidelity to currently accepted anatomical models would dictate using L-III(2) as the output port. However, since the axonal arborization of layer 6 pyramidal cells made in layer 4 shows a diameter of 590 μm (Douglas and Martin, 2004), it is at least plausible to use L-VI as the projection port to adjacent columns. To model cortico-cortical projections over greater distances one would use group 1 L-III(1) or L-III(2) as the projecting output port since the high-frequency gamma-band signals are preserved there in β-BPF columns.

Figure 4. Response of γ-HPF Column to 28 Hz input applied to N1 and synchronous 27 Hz inputs applied to N2-N4. The time is in milliseconds. The exact signaling periods are 35 msec and 37 msec, respectively. The figure shows, in order from top to bottom, L-IV, L-III(1), and L-III(2). The y-axis labels are neuron numbers as defined in figure 1. Column output kernel L-VI is the same as L-III(2) delayed by 1 msec.

Figure 5. Response of γ-HPF chain columns 2 and 3 to column 1 outputs. (a) Response of column 2 kernels L-IV, L-III(1), and L-III(2). (b) Response of column 3 kernels L-IV, L-III(1), and L-III(2). The time is in milliseconds. The order of the kernels in the figure is top to bottom. The first column receives the synchronous inputs from column 1 kernel L-VI shown in figure 4. The second column receives synchronous inputs from kernel L-VI of column 2. Column 2 L-VI tracks column 2 kernel L-III(2) with 1 msec delay; column 3 L-VI tracks column 3 L-III(2) with 1 msec delay.

Figure 6. Packeting in the response of γ-HPF chain in column 1 driven by pairs of synchronous inputs at different frequencies. The synchronous inputs to N1-N2 have a 22 msec period; the inputs to N3-N4 have a 21 msec period. The time is in milliseconds. The pulse period in the first packet ($t < 300$ msec) is 21 msec. The pulse period in the second packet is 22 msec. From top to bottom, the kernels shown are L-IV, L-III(1), and L-III(2). The output kernel L-VI tracks L-III(2) with a 1 msec delay. Transmission in a chain of columns is evanescent due to integrator loss.

Figure 7. β-BPF chain response in column 1 group 1 to synchronous 27 Hz inputs. From top to bottom the kernels are L-IV, L-III(1), L-III(2), L-V(1), L-V(2), and L-VI. Note that L-VI does not follow L-III(2) in β-BPF group 1 due to inhibitory feedback from group 2. The time is in milliseconds. The transmission of the synchronous output pulses (N26-N29) in the chain is evanescent due to integrator loss. Column 4 in the chain never receives any input from the upstream columns.

Figure 8. Response of column 1 group 2 kernels L-IV, L-III(1), and L-III(2) to the assembly being driven by synchronous 27 Hz inputs into group 1. The time is in milliseconds. The kernels are ordered top to bottom in the figure from L-IV to L-III(2). L-III(2) inhibitory neuron N45 projects to kernels L-V(1), L-V(2), L-VI of group 1 in the assembly. Group 2 kernels L-V(1) and L-V(2) track L-III(2). Group 2 kernel L-VI tracks L-III(2) with a 1 msec delay. L-III(1) controls the firing of these other kernels. L-III(2) through L-VI fire at half the rate of L-III(1) due to inhibition by their local inhibitory neurons. L-III(1) does not have this response because its synaptic weights from L-IV are larger by a factor of 3 than are the synaptic weights for projection from L-III(1) to L-III(2), L-V(1), and L-V(2) and from L-V(1) to L-VI. This allows L-III(1) to overcome the effects of inhibition at the time of its second, fourth, etc. pulses. The downstream kernels, on the other hand, do not have enough excitation to overcome inhibition at these times. This is one mechanism for subharmonic generation in the assembly.

Figure 9. Induction of RM mode firing in β-BPF column 1 group 1 by asynchronous inputs with periods 52, 50, 47, and 49 msec. This dynamic produces traveling waves in the form of closely spaced dipulses. The time is in milliseconds. From top to bottom the kernels are L-IV, L-III(1), L-III(2), L-V(1), L-V(2), and L-VI. The L-VI dipulses are located at approximately 100 and 800 msec. The other L-VI pulses are singletons and are absorbed by integrator loss in column 2.

Figure 10. Induction of RM mode in β-BPF column 2 group 1 driven by the cell group in figure 9. From top to bottom the kernels are L-IV, L-III(1), L-III(2), L-V(1), L-V(2), and L-VI. The time is in milliseconds. The column produces dipulse outputs at just past $t = 100$ and $t = 800$. The singleton pulses output by column 1 are absorbed by integrator loss. The output of this column induces RM mode operation in the next, and so on, leading to traveling wave dipulse propagation.

Figure 11. Fourier magnitude spectrum of β-BPF chain operating in RM mode. The output signals of all 180 neurons in the chain were summed and the Fourier magnitude computed using the Fast Fourier Transform. This is meant to mimic what might be observed by an ideal probe placed at this area of the cortex. The input signals to the chain were at 19, 20, 21, and 22 Hz (middle of the beta-band). The chain produces subharmonics in the low- and alpha-band regions and generates gamma-band spectral components. The input signals are not included in this calculation. The network generates only a small amount of energy in the beta-band.

Table (note: the table is done as text in Word with tab spacing 0.1" and 9-pt font.)

Table 1. Values of synaptic weight constants *w* for excitatory projections within a cell group. All cell groups use the same constants.

	Source					
	L-IV	L-III(1)	L-III(2)	L-V(1)	L-V(2)	L-VI
L-IV						
EN						0.25
IN	0.95					0.05
L-III(1)						
EN	0.75		0.25			
IN	.025	0.95	.025			
L-III(2)						
EN		0.25			0.25	
IN		.025	0.95		.025	
L-V(1)						
EN		0.25			0.25	
IN		.025		0.95	.025	
L-V(2)						
EN		0.25		0.25		
IN		.025		.025	0.95	
L-VI						
EN				0.75		
IN				.025		0.95

Figures

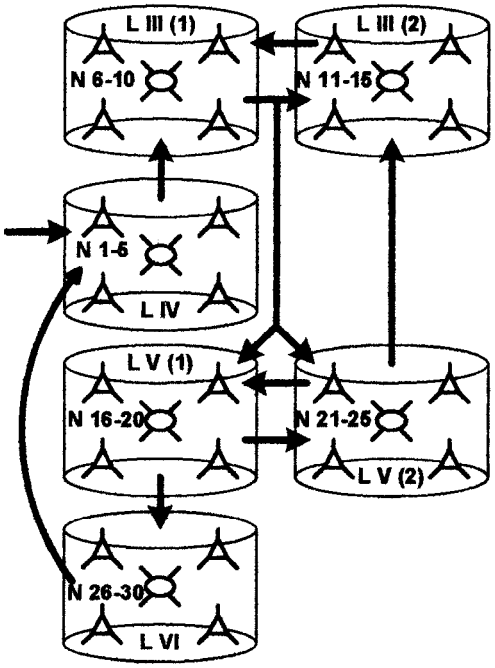

Figure 1

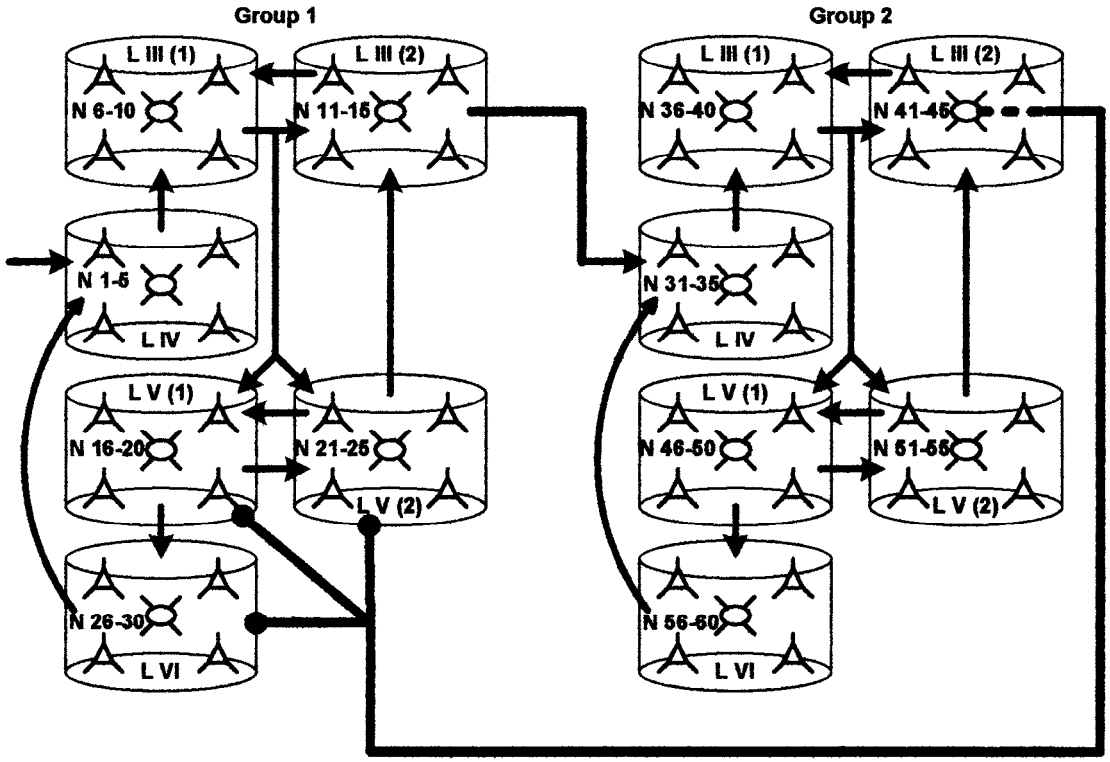
Group 1
Group 2
L III (1)
L III (2)
N 6-10
N 11-15
N 36-40
N 41-45
N 1-5
L IV
N 31-35
L IV
L V (1)
L V (2)
N 16-20
N 21-25
N 46-50
N 51-55
L V (2)
N 26-30
L VI
N 56-60
L VI

Figure 2

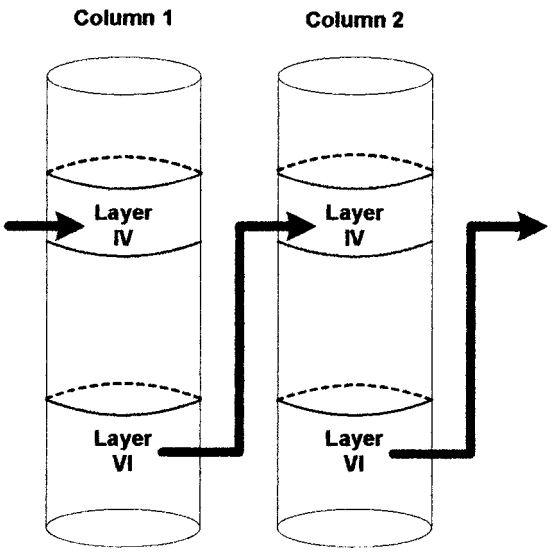

Figure 3

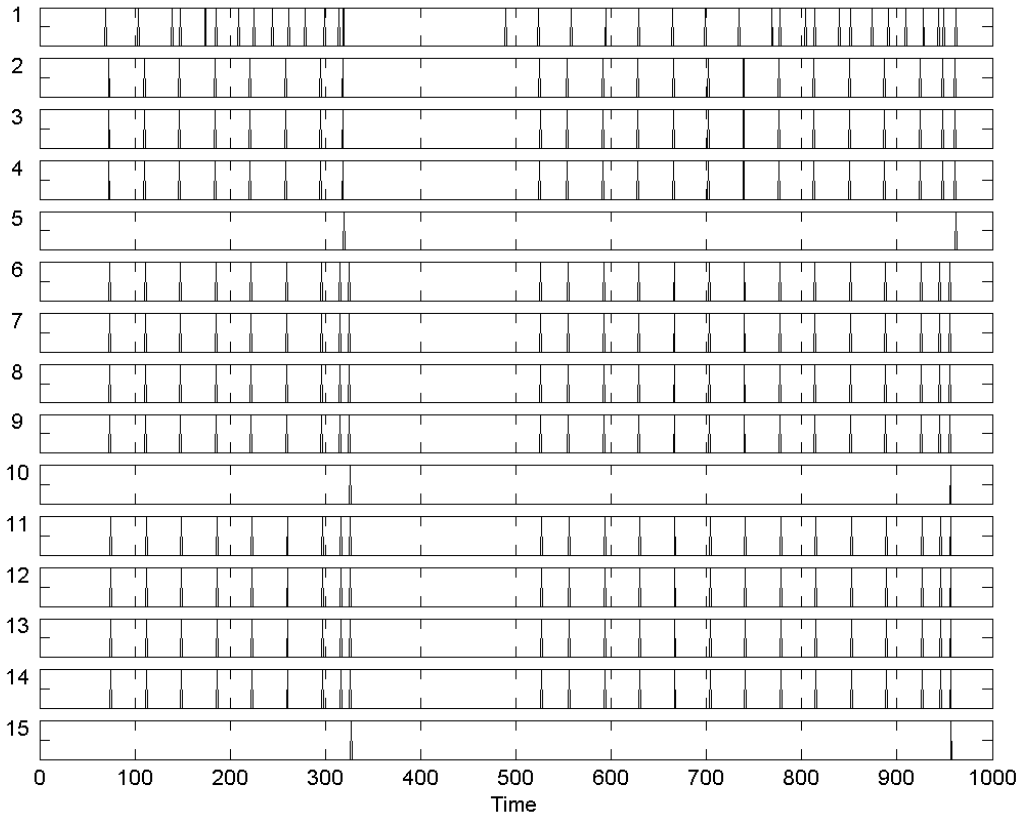
1
2
3
4
5
6
7
8
9
10
11
12
13
14
15
0
100
200
300
400
500
600
700
800
900
1000
Time

Figure 4

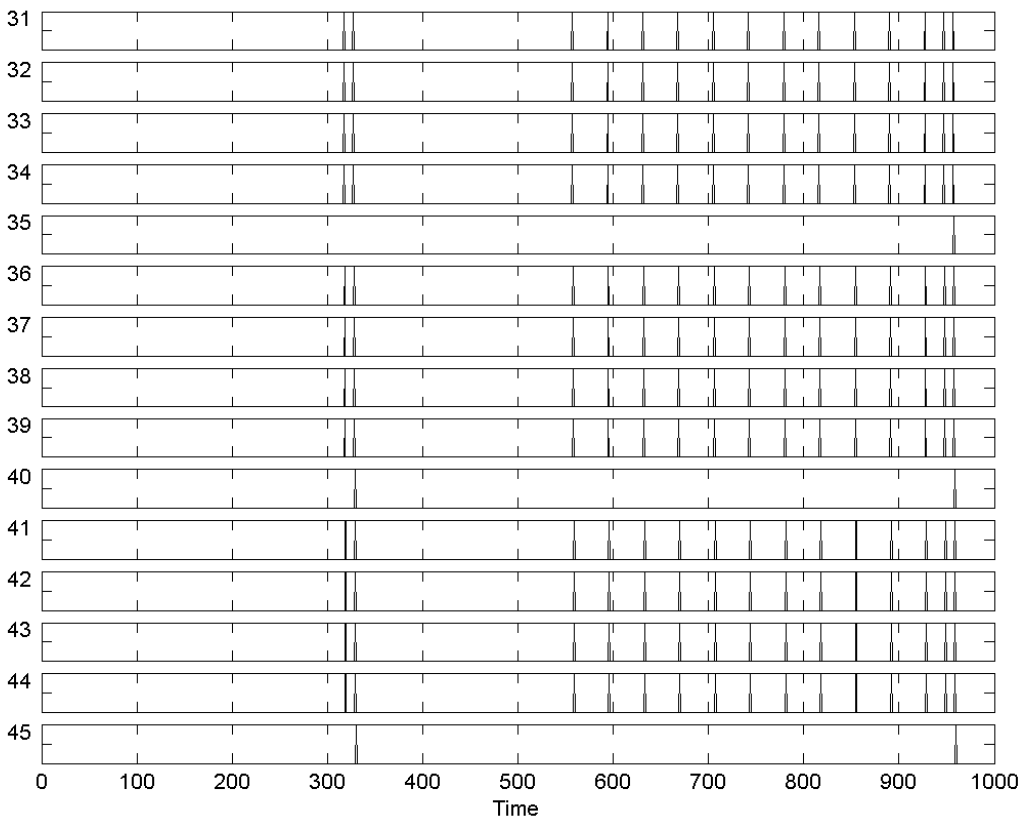
31
32
33
34
35
36
37
38
39
40
41
42
43
44
45
0
100
200
300
400
500
600
700
800
900
1000
Time

Figure 5(a)

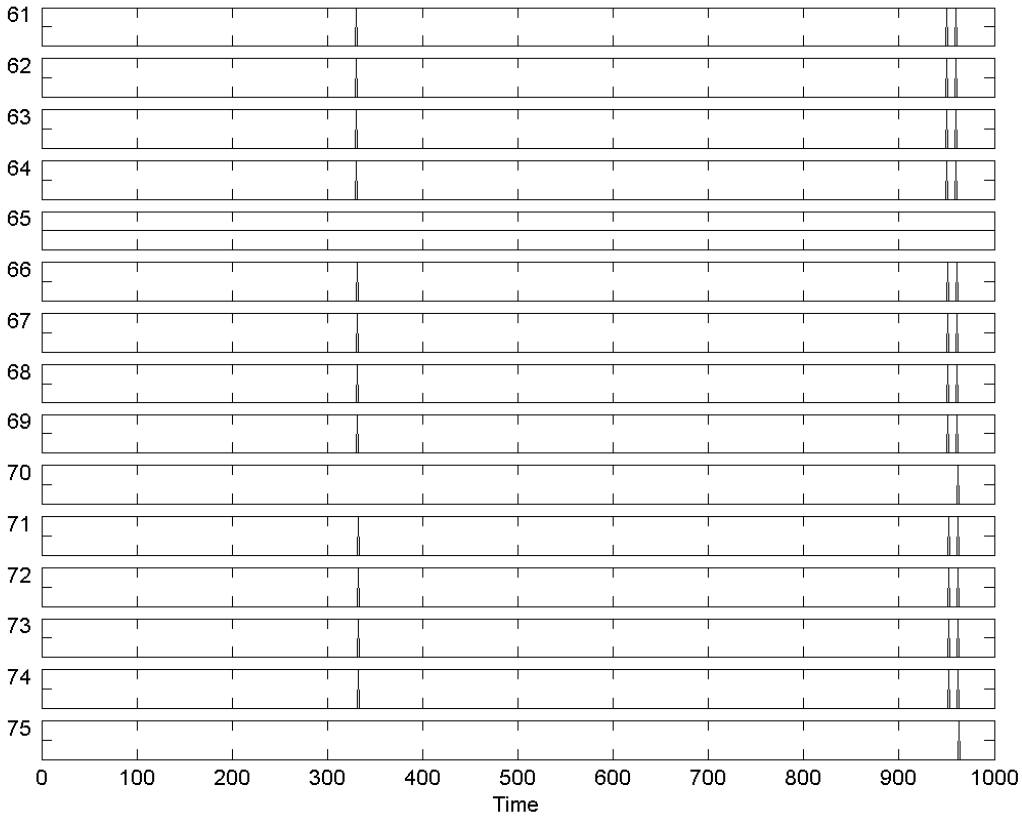
61
62
63
64
65
66
67
68
69
70
71
72
73
74
75
0
100
200
300
400
500
600
700
800
900
1000
Time

Figure 5(b)

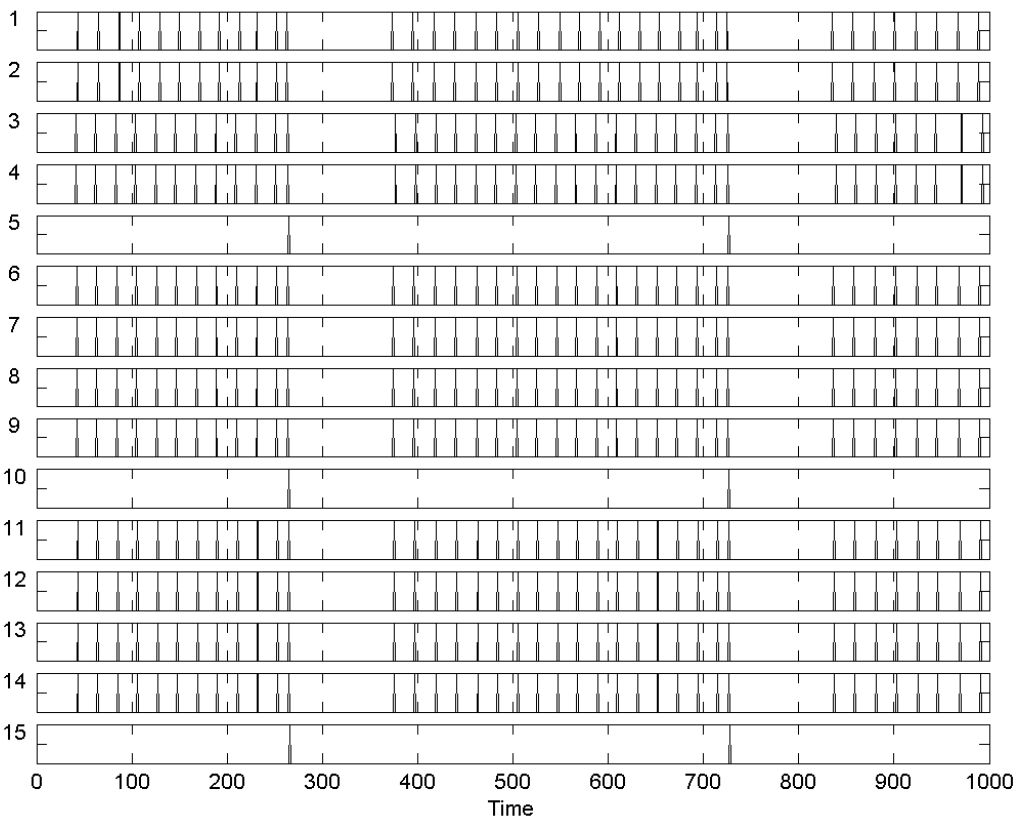
1
2
3
4
5
6
7
8
9
10
11
12
13
14
15
0
100
200
300
400
500
600
700
800
900
1000
Time

Figure 6

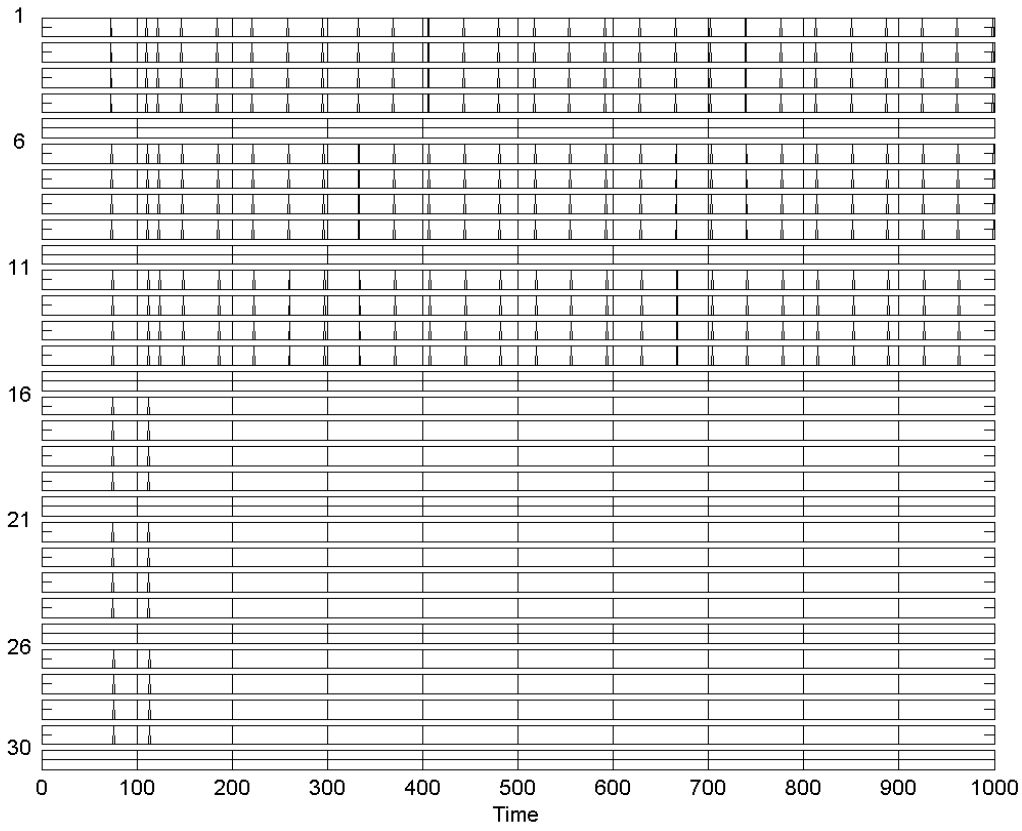

Figure 7

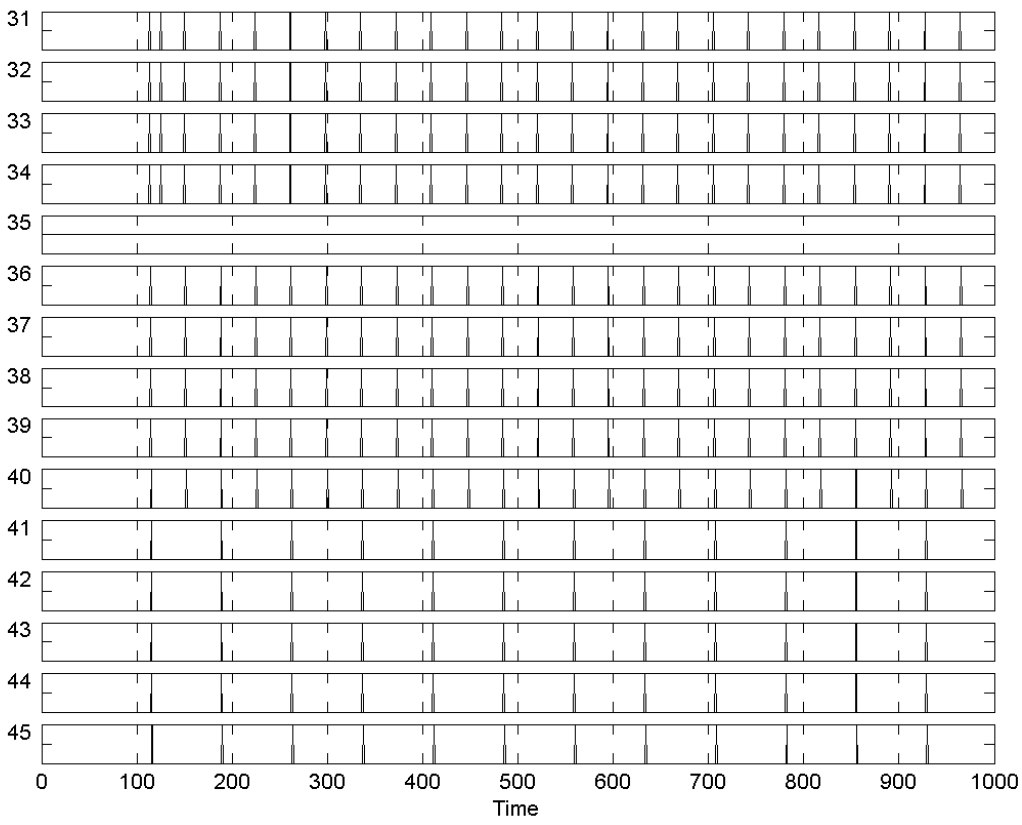
31
32
33
34
35
36
37
38
39
40
41
42
43
44
45
0
100
200
300
400
500
600
700
800
900
1000
Time

Figure 8

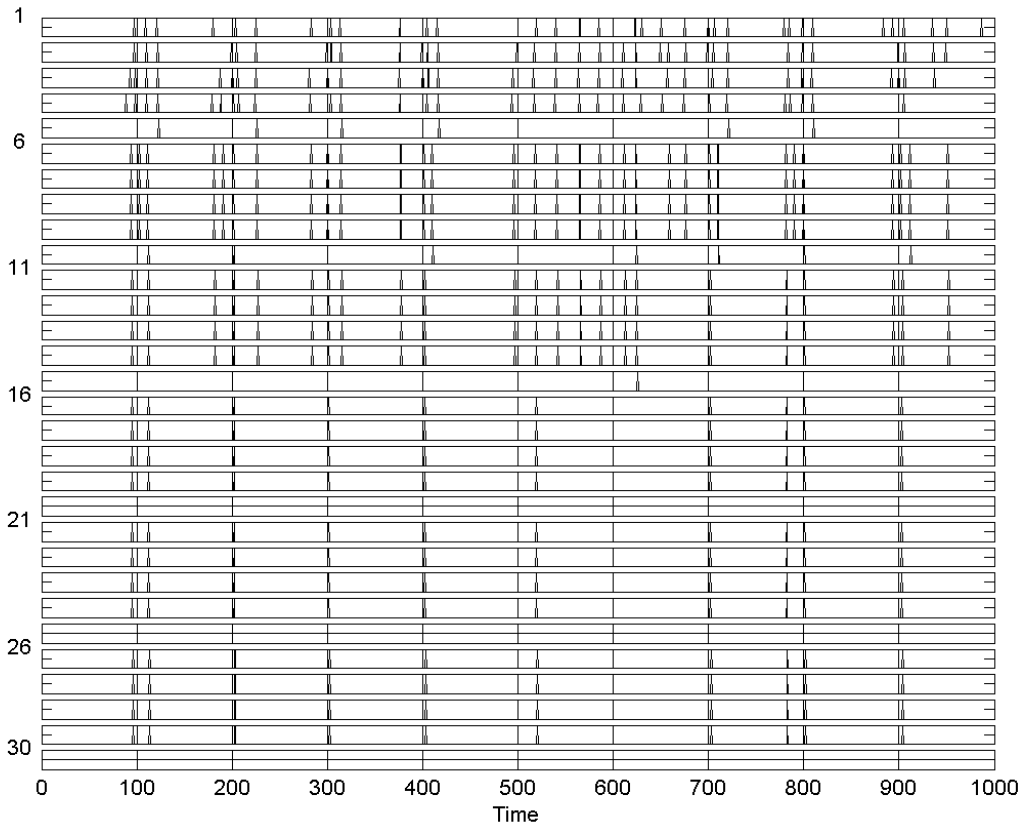

Figure 9

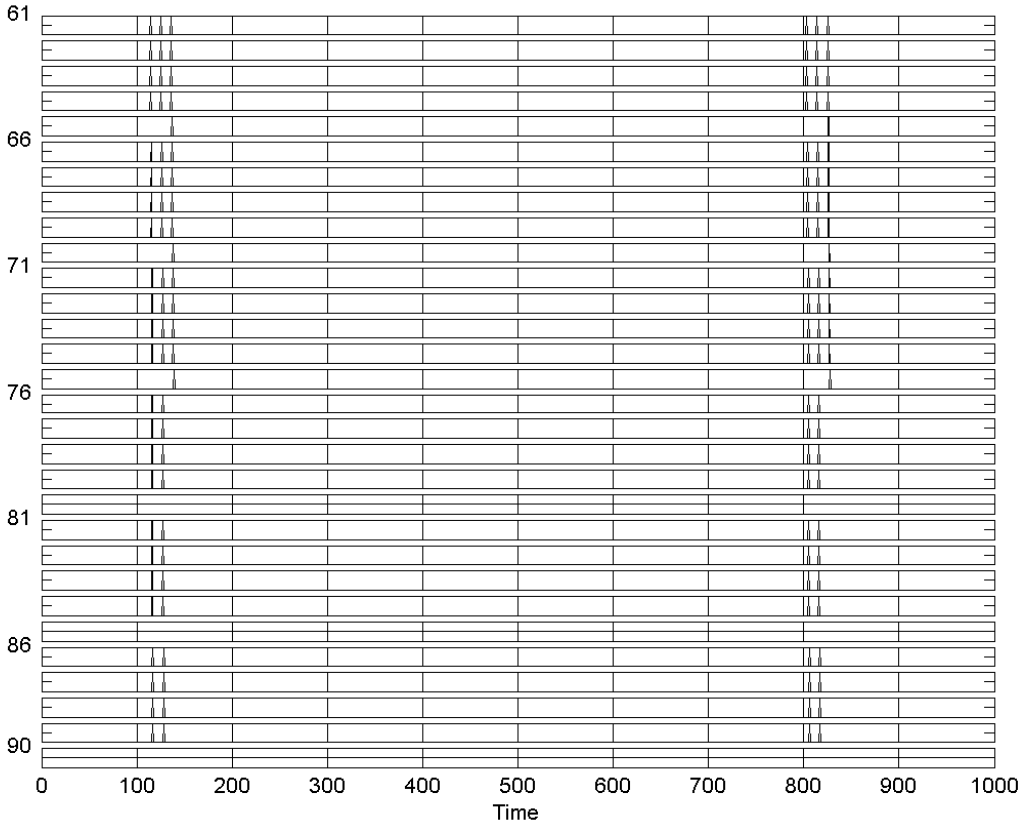
61
66
71
76
81
86
90
0
100
200
300
400
500
600
700
800
900
1000
Time

Figure 10

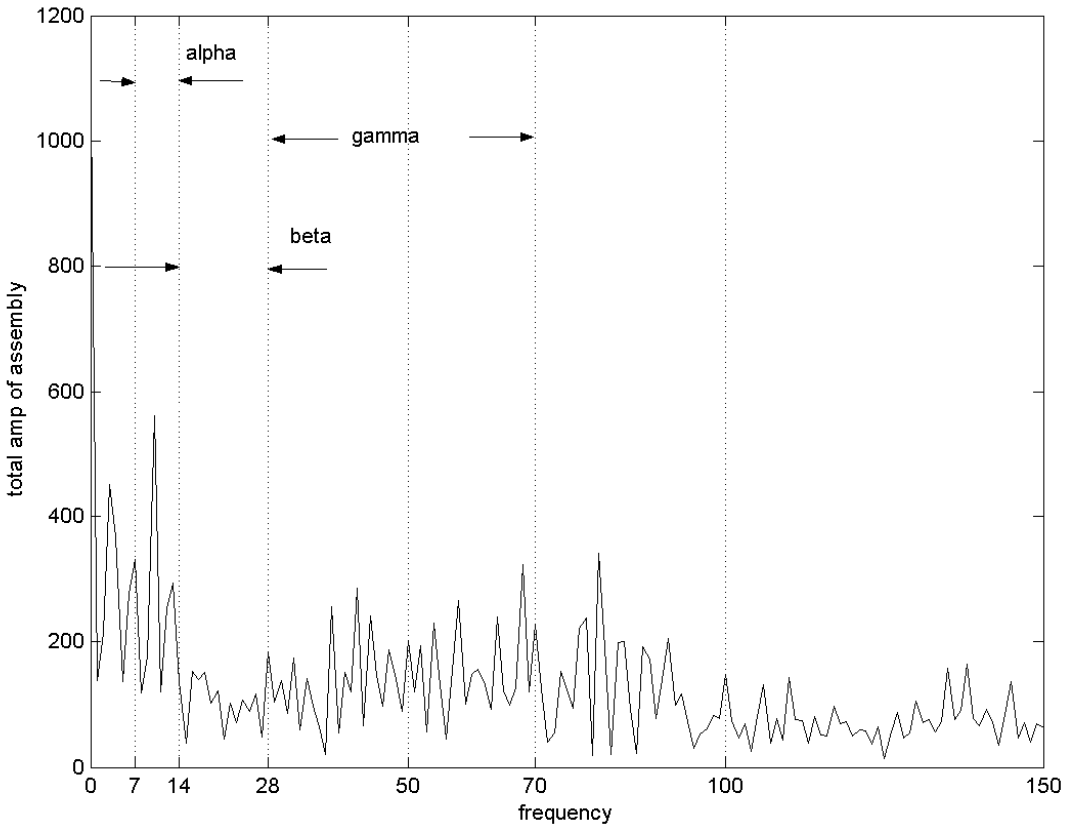
1200
1000
800
600
400
200
0
alpha
gamma
beta
total amp of assembly
0
7
14
28
50
70
100
150
frequency

Figure 11

A. Appendix

A.1 Synaptic Weights within a Cell Group

Kernel-to-kernel synapses use equal-valued synaptic weights w for the feeding field input of the excitatory dendrites. Letting Y denote a column vector of the four inputs y_k received from the source kernel, the feeding field input is given by

$$\sum_k w_k y_k = w\begin{bmatrix}1 & 1 & 1 & 1\end{bmatrix}Y \, .$$

Table 1 gives the w values for the kernel interconnections.

Table 1 (width = 3" at 9-pt. font)

The synaptic weight for the inhibitory dendrite feeding field input for feedback connections within a kernel is $w = 1$. The linking field weight for the excitatory dendrite of an EN is $w = 1$ if the source neuron is a nearest neighbor (refer to figure 1) and $w = 0.5$ if the source is not a nearest neighbor. No neuron feeds back to its own linking field.

A.2 Synaptic Weights for Column and Group Inputs

Column 1 group 1 receives the external input signals to the HPF or BPF chain at kernel L-IV. Let x_k denote the weighted input to the k^{th} neuron in L-IV of column 1 group 1. For all simulations reported in this paper these weighted inputs are given by

$$\begin{bmatrix}x_1\\x_2\\x_3\\x_4\end{bmatrix} = \begin{bmatrix}1 & 0 & 0 & 0\\0 & 1 & 0 & 0\\0 & 0 & 1 & 0\\0 & 0 & 0 & 1\end{bmatrix}\begin{bmatrix}s_1\\s_2\\s_3\\s_4\end{bmatrix}$$

where s_k is the k^{th} input signal. For all other L-IV inputs the synaptic weighting is given by

$$\begin{bmatrix}x_1\\x_2\\x_3\\x_4\end{bmatrix} = \begin{bmatrix}0.25 & 0.25 & 0.25 & 0.25\\0.25 & 0.25 & 0.25 & 0.25\\0.25 & 0.25 & 0.25 & 0.25\\0.25 & 0.25 & 0.25 & 0.25\end{bmatrix}\begin{bmatrix}y_1\\y_2\\y_3\\y_4\end{bmatrix}$$

where y_k is the k^{th} EN output in the kernel feeding the group input port L-IV. When a neuron fires $y_k = 1$; otherwise $y_k = 0$.

In the BPF column, group 1 receives feedback from the inhibitory neuron in L-III(2) of group 2. We used a single large value, $w = 10$, for the weighting. This connection requires some explanation. The nature of the horizontal connections made by inhibitory neurons in neocortex is not as yet well known.

It is presently accepted that large basket cells in cortical layers 3 and 5 make longer-range connections within their layers to pyramidal cells (Martin and Douglas, 2004). This is possibly the case for layer 6 basket cells as well (White, 1989B). There is some evidence to suggest that at least some basket cells probably have a higher synaptic efficacy, judging from the IPSPs they produce, compared to excitatory synapses (Gibson and Connors, 2003). A liberal albeit very problematical interpretation of these reports could argue in favor of feeding back the IN outputs of all the kernels except L-IV, each with a synaptic weight factor $w = 2$. However, because the kernels in group 2 of the BPF column tend to fire almost synchronously with a phase delay of at most ±1 msec relative to L-III(2) and because it seems to us of little value to put in specific kernel-to-kernel connections where the anatomical and physiological data on neocortical organization does not exist to support the model accuracy such specificity tends to imply, we elected to merely clump all group-to-group inhibitory feedback at one point and apply Wang's rule to determine the effective value of w. Put another way, we do not know the proper biological connectivity for the inhibitory feedback and we decided to let the model loudly announce this fact.

A.3. Neuron Parameters

The excitatory neurons for the β-HPF group for all kernels except L-IV have the same parameters. They are: $V_{fe} = 0.6$; $\tau_{fe} = 5$; $V_{\lambda} = 5$; $\tau_{\lambda} = 0.5$; $V_{fi} = 5$; $\tau_{fi} = 15$; $\theta_0 = 0.5$; $V_s = 80$; $\tau_s = 1.55$. The excitatory L-IV parameters are: $V_{fe} = 0.6$; $\tau_{fe} = 15$; $V_{\lambda} = 5$; $\tau_{\lambda} = 0.5$; $V_{fi} = 5$; $\tau_{fi} = 10$; $\theta_0 = 0.606$; $V_s = 80$; $\tau_s = 1.55$. The inhibitory neuron parameters are: $V_{fe} = 0.06$; $\tau_{fe} = 30$; $\theta_0 = 0.5$; $V_s = 80$; $\tau_s = 3.5$ for all kernels.

The excitatory neurons in the γ-HPF group used in the β-BPF column all have the same parameters except for θ_0 in the L-IV kernel. For the L-IV kernel $\theta_0 = 0.60035$; for the other kernels $\theta_0 = 0.5$. The other parameters are: $V_{fe} = 0.6$; $\tau_{fe} = 5$; $V_{\lambda} = 5$; $\tau_{\lambda} = 0.5$; $V_{fi} = 5$; $\tau_{fi} = 15$; $V_s = 80$; $\tau_s = 1.55$. The parameters for the inhibitory neuron in L-IV are: $V_{fe} = 0.08$; $\tau_{fe} = 20$; $\theta_0 = 0.5$; $V_s = 80$; $\tau_s = 3.5$. The inhibitory neuron parameters for the other kernels are: $V_{fe} = 0.15$; $\tau_{fe} = 20$; $\theta_0 = 0.5$; $V_s = 80$; $\tau_s = 3.5$.

The excitatory neurons in the γ-HPF used as a functional column in a γ-HPF chain have the same parameters as the other γ-HPF except for θ_0 in L-IV. The L-IV $\theta_0 = 0.60038$. All the inhibitory neurons have the same parameters. They are: $V_{fe} = 0.08$; $\tau_{fe} = 20$; $\theta_0 = 0.5$; $V_s = 80$; $\tau_s = 3.5$.

All neurons have a built-in 1 msec delay from input to output. The simulation time step was 1 msec and the neuron equations were appropriately converted for simulation to difference equations for this time step.